AD-A146 339 MILLIMETER-WAVE PROPAGATION AND REMOTE SENSING OF THE ATMOSPHERE(U) ROME AIR DEVELOPMENT CENTER GRIFFISS AFB NY E E ALTSHULER DEC 83 RADC-RR-83-297 1/1

UNCLASSIFIED F/G 4/1 NL

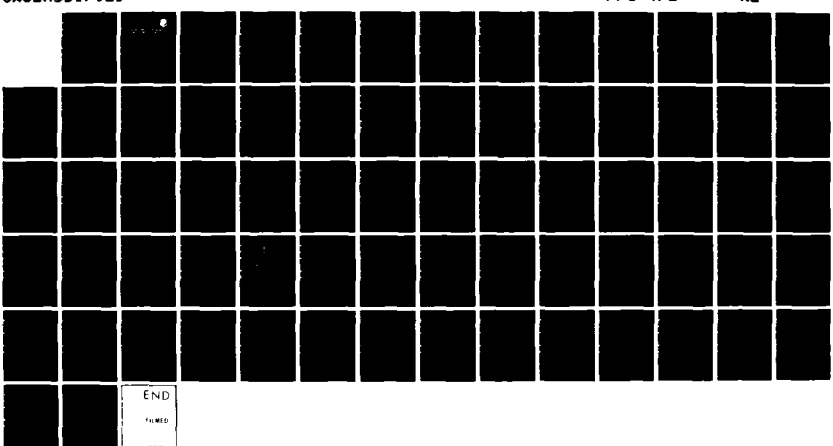

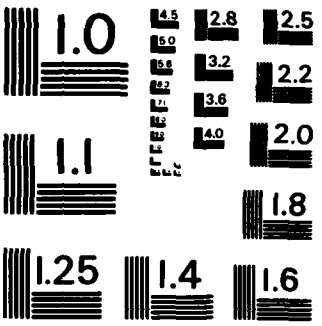

(12)

AD-A146 339

RADC-TR-83-297
In-House Report
December 1983

MILLIMETER-WAVE PROPAGATION AND REMOTE SENSING OF THE ATMOSPHERE

Edward E. Altshuler

APPROVED FOR PUBLIC RELEASE; DISTRIBUTION UNLIMITED

DTIC FILE COPY

ROME AIR DEVELOPMENT CENTER
Air Force Systems Command
Griffiss Air Force Base, NY 13441

This report has been reviewed by the RADC Public Affairs Office (PA) and is releasable to the National Technical Information Service (NTIS). At NTIS it will be releasable to the general public, including foreign nations.

RADC-TR-83-297 has been reviewed and is approved for publication.

APPROVED: John E Rasmussen

JOHN E. RASMUSSEN
Chief, Propagation Branch
Electromagnetic Sciences Division

APPROVED: Allan C. Schell

ALLAN C. SCHELL
Chief, Electromagnetic Sciences Division

APPROVED: John A. Ritz

JOHN A. RITZ
Acting Chief, Plans Office

If your address has changed or if you wish to be removed from the RADC mailing list, or if the addressee is no longer employed by your organization, please notify RADC (EEPS), Hanscom AFB MA 01731. This will assist us in maintaining a current mailing list.

Do not return copies of this report unless contractual obligations or notices on a specific document requires that it be returned.

Unclassified

SECURITY CLASSIFICATION OF THIS PAGE (When Data Entered)

REPORT DOCUMENTATION PAGE		READ INSTRUCTIONS BEFORE COMPLETING FORM
1. REPORT NUMBER RADC-TR-83-297	2. GOVT ACCESSION NO. AD-A146 357	3. RECIPIENT'S CATALOG NUMBER
4. TITLE (and Subtitle) MILLIMETER-WAVE PROPAGATION AND REMOTE SENSING OF THE ATMOSPHERE		5. TYPE OF REPORT & PERIOD COVERED In-House 6. PERFORMING ORG. REPORT NUMBER
7. AUTHOR(s) Edward E. Altshuler		8. CONTRACT OR GRANT NUMBER(s)
9. PERFORMING ORGANIZATION NAME AND ADDRESS Rome Air Development Center (EEPS) Hanscom AFB Massachusetts 01731		10. PROGRAM ELEMENT, PROJECT, TASK AREA & WORK UNIT NUMBERS 62702F 46001607
11. CONTROLLING OFFICE NAME AND ADDRESS Rome Air Development Center (EEPS) Hanscom AFB Massachusetts 01731		12. REPORT DATE December 1983 13. NUMBER OF PAGES 67
14. MONITORING AGENCY NAME & ADDRESS(if different from Controlling Office)		15. SECURITY CLASS. (of this report) Unclassified 15a. DECLASSIFICATION/DOWNGRADING SCHEDULE N/A

16. DISTRIBUTION STATEMENT (of this Report)

Approved for public release; distribution unlimited.

17. DISTRIBUTION STATEMENT (of the abstract entered in Block 20, if different from Report)

18. SUPPLEMENTARY NOTES

RADC Project Engineer: Edward E. Altshuler, RADC/EEPS
Reprint of Chapter 4 of Infrared and Millimeter Waves, Vol. 9, (1983) Academic Press, Inc.

19. KEY WORDS (Continue on reverse side if necessary and identify by block number)

Millimeter wavelengths
Propagation effects
Remote sensing of atmosphere

20. ABSTRACT (Continue on reverse side if necessary and identify by block number)

The propagation characteristics in the millimeter-wave region of the spectrum are of particular interest because the waves have a strong interaction with lower atmospheric gases and particulates. The effects of this interaction are twofold: on the other hand, atmospheric absorption, scattering and refraction limit the performance of millimeter-wave systems; on the other hand, this interaction allows the propagated wave to be used as a diagnostic tool to probe lower atmospheric structure.

DD FORM 1 JAN 73 1473 EDITION OF 1 NOV 65 IS OBSOLETE

Unclassified

SECURITY CLASSIFICATION OF THIS PAGE (When Data Entered)

20. (Contd)

The principal applications of millimeter waves have been in the areas of communications, radar, and remote sensing. The availability of large bandwidths makes this region of the spectrum particularly attractive for high data rate communications. Because the angular resolution of an aperture is inversely proportional to wavelength, higher resolution antennas are achievable at millimeter waves than at longer wavelengths. Furthermore, because range resolution is a function of bandwidth, improved range resolution is also possible. With this enhanced resolution, higher-precision radard for tracking, guidance, mapping, and target detection are now realizable. High-gain, high-resolution antennas of moderate size and lightweight, compact system components are indeed applicable for space vehicle instrumentation. In the area of remote sensing atmospheric structure is being probed using both ground-based and space-based active and passive systems.

The effects of atmospheric gases and particulates on millimeter-wave systems are reviewed. For the clear atmospheric, absorption due to oxygen and water vapor is of principal concern, however, refraction, scattering, diffraction and depolarization effects may also be present. For an atmosphere containing particulates, absorption, scattering and depolarization by rain seriously limit propagation at millimeter wavelengths. In general, atmospheric effects become more severe as the wavelength become shorter, so most systems are currently operating at longer millimeter wavelengths.

Contents

Illustrations

Millimeter-Wave Propagation and Remote Sensing of the Atmosphere

I. Introduction

The propagation characteristics of electromagnetic waves in the millimeter-wave region of the spectrum are of particular interest because the waves have a strong interaction with lower atmospheric gases and particulates. The effects of this interaction are twofold: on the one hand, atmospheric absorption, scattering, and refraction limit the performance of millimeter-wave systems; on the other hand, this interaction allows the propagated wave to be used as a diagnostic tool to probe lower atmospheric structure.

Millimeter waves are generally considered to cover wavelengths in the range from about 2 cm down to 1 mm (15–300 GHz). These limits are based both on wavelength and on the nature and magnitude of the interaction between the wave and the atmosphere. Although the interaction with the atmosphere does not change abruptly at these limits, it does become

(Received for publication 9 January 1984)

weaker at longer wavelengths and stronger at shorter wavelengths. Thus the concepts presented here can generally be extended to either slightly longer or slightly shorter wavelengths. We shall often refer to the "window regions" of the millimeter-wave spectrum. These are considered the low attenuation regions between the gaseous absorption resonances. In particular, wavelengths between the 1.35-cm water vapor resonance and 5-mm oxygen resonance, the 5- and 2.5-mm oxygen resonances, and the 2.5-mm oxygen resonance and 1.6-mm water vapor resonance compose the window regions. Low attenuation regions also exist at wavelengths longer than 1.35 cm and shorter than 1.6 mm.

The physics of the interaction between millimeter waves and the atmosphere is extremely complex, so many facets are considered beyond the scope of this book. However, an effort is made to provide the reader with a general understanding of the mechanisms of this interaction; if in-depth details are required, they can be obtained from the references. Likewise, complex mathematical expressions are used only to illustrate concepts that are considered important and cannot be satisfactorily explained otherwise. Many of the figures contain information that is "typical" or "average," that is, it is intended to provide the reader with an estimate of the magnitude of an interaction. More quantitative results are available from the cited references.

A. Propagation Effects

Atmospheric gases and particulates often have a profound effect on millimeter waves and thus limit the performance of many millimeter-wave systems. Because the densities of these gases and particulates generally decrease with altitude, the effects of the atmosphere on the propagated wave are strongest very close to the earth and tend to diminish at higher altitudes. For this reason millimeter waves propagating above the tropopause, the altitude at which the temperature remains essentially constant with increasing height ($\sim 10-12$ km), are assumed to be unaffected. For the clear atmosphere there are essentially two types of interactions. The stronger interaction is the absorption–emission produced by oxygen and water vapor. The other interaction takes place with the refractivity structure of the atmosphere. This refractivity structure is often divided into two categories: gross structure and fine structure. The gross structure assumes the atmosphere is a horizontally stratified continuum characterized by a refractivity that normally decreases slowly with increasing altitude, and is assumed to be wavelength independent; that is, it affects all wavelengths from microwaves through millimeter waves in the same way. For the refractivity fine structure, the atmosphere is viewed as an inhomogeneous medium consisting of small pockets of refractive index that vary both temporally and spatially.

Because these pockets have different sizes, this interaction is wavelength dependent. Although the terrain is not actually part of the atmosphere, it does interface with the atmosphere and can affect millimeter-wave propagation. Thus, multipath propagation produced by the terrain and diffraction by prominent obstacles on the earth's surface are also reviewed.

Atmospheric particulates range in size from microns to close to 1 cm in diameter. For particles very small compared to wavelength, the only significant propagation effects are those of absorption and emission. As the particles become larger with respect to wavelength, scattering effects become pronounced. In Section II we shall review the effects of the clear atmosphere and then of atmospheric particulates on millimeter-wave propagation. We show that although the effects of the clear atmosphere are generally not as severe as those due to atmospheric particulates, they cannot be disregarded, even in the window regions and especially at short millimeter wavelengths.

B. Remote Sensing

Because millimeter waves are strongly affected by both atmospheric gases and particulates, which are in turn a function of the meteorological properties of the atmosphere, it is possible to obtain meteorological information by observing the behavior of the propagated wave. This technique was first employed at IR wavelengths and proved very successful for clear sky conditions. At IR, however, atmospheric particulates such as cloud or fog tend to mask out parameters of interest and thus limit the use of IR for remote sensing during overcast conditions. Millimeter waves are less affected by cloud and fog, so it is still possible to infer information on, for example, temperature and water vapor under adverse weather conditions. Three techniques for remotely sensing the atmosphere are reviewed: line-of-sight transmission, radiometry, and radar. Similar millimeter-wave sensors have been used to probe the earth and ocean; however, these applications are considered separate from the atmosphere and are not addressed in this chapter.

C. Applications

Potential applications of millimeter waves have been considered for many years (Altshuler, 1968; Skolnik, 1970). However, for most applications other than remote sensing, atmospheric effects have always imposed limitations on system performance. The principal applications of millimeter waves have been in the areas of communications, radar, and remote sensing. Probably the first application for which millimeter waves were considered was communications. The discovery of the circular electric waveguide mode TE_{01} about four decades ago prompted the use of these wavelengths for a waveguide communication system, because waveguide attenuation for that

mode decreases with decreasing wavelength. It is believed that the most significant contribution resulting from this effort was not so much the system itself but the research that was directed toward the development of a whole new line of millimeter-wave equipment and techniques required for this application — i.e., sources, amplifiers, detectors, and waveguide components. Through the years consideration was often given to utilizing millimeter waves for point-to-point communications. However, proposed systems never materialized, principally because they were not economically competitive with those at longer wavelengths; they also lacked reliability because of atmospheric effects and inferior components.

In the past decade, the need for new types of communication systems and the need to alleviate increasing spectrum congestion have led to a reappraisal of millimeter waves. The availability of large bandwidths makes this region of the spectrum particularly attractive for high data rate earth-to-space communication channels. Furthermore, high-gain, high-resolution antennas of moderate size and light-weight, compact system components are indeed applicable for space vehicle instrumentation. Millimeter waves provide an excellent means for obtaining secure communication channels. For satellite-to-satellite links, where all propagation is above the absorptive constituents of the lower atmosphere, narrow-beamwidth antennas may be operated at a wavelength where atmospheric attenuation is very high (i.e., $\lambda \sim 5$ mm); thus the signal is confined by the antenna to a narrow cone and then absorbed by the lower atmosphere before it reaches the earth. Another application for secure communications is ship-to-ship and short terrestrial links; in these cases attenuation is sufficiently high at millimeter waves to allow a detectable signal only over short distances. Finally, point-to-point radio-relay systems that were previously not considered feasible are now being reexamined. Recent studies have shown that attenuation in the lower atmosphere can be combatted by using very short hops and diversity techniques; also, satisfactory system performance can now be obtained with solid-state components quite economically.

Because the angular resolution of an aperture is inversely proportional to wavelength, antennas can have higher resolution at millimeter wavelengths than at longer wavelengths. Furthermore, because range resolution is a function of bandwidth, improved range resolution is also possible. With this enhanced resolution, higher-precision radars for tracking, guidance, mapping, and target detection are now realizable. As in the case of communications, millimeter-wave radars also have far-reaching applications for aircraft and spacecraft because of the high resolution that can be obtained with relatively compact systems.

In the area of remote sensing there are numerous applications for millimeter-wave sensors. Although in this chapter we address only remote

sensing of the atmosphere, millimeter-wave sensors also have application in geology, hydrology, agriculture, oceanography, and astronomy.

An attempt has been made to identify most of the applications for which millimeter waves are being considered, and the future looks bright. Furthermore, it must be remembered that in any emerging field the benefits derived from unforeseen applications often outweigh the benefits initially foreseen.

II. Atmospheric Effects on Propagated Waves

Atmospheric gases and particulates may severely alter the properties of millimeter waves. For the clear atmosphere the most pronounced effect is absorption due to the gases, oxygen and water vapor. However, refraction, scattering, diffraction, and depolarization effects are also reviewed, and it is shown that under special conditions their impact on the propagated wave can be significant. For an atmosphere containing particulates, the absorption and scattering by rain seriously limit propagation at millimeter wavelengths. However, the effects of smaller, water-based particulates are also significant, particularly at shorter millimeter wavelengths.

A. Clear Atmosphere

We shall consider an atmosphere "clear" if it is free of atmospheric particulates. Thus the only interaction that takes place is that between the propagated wave and the atmospheric gases (and terrain). We shall see that for very low elevation angles the gross structure of the refractive index causes the propagated wave to be bent and delayed, whereas the fine structure of the refractive index scatters the propagated wave and may produce scintillations. The gases, oxygen and water vapor, absorb energy from the wave and reradiate this energy in the form of noise. Finally, if the wave is propagating close to the earth's surface, part of the energy may be reflected from the surface, or it may be diffracted by prominent obstacles on the surface and then interfere with the direct signal. If some form of reflection or scattering takes place, the propagated wave may also become depolarized. All of these effects are discussed in detail in Sections II.A.1–II.A.5.

1. *Refraction*

The lower atmosphere is composed of about 78% nitrogen, 21% oxygen, and 1% water vapor, argon, carbon dioxide, and other rare gases. The densities of all these gases, except for water vapor, decrease gradually with height; the density of water vapor, on the other hand, is highly variable. The index of refraction of the atmosphere is a function of the temperature, pressure, and partial pressure of water vapor. Because the refractive index n

is only about 1.0003 at the earth's surface, it is often expressed in terms of a refractivity N, where

$$N = (n - 1) \times 10^6. \tag{1}$$

The radio refractivity can be approximated by the following theoretical expression, which has empirically derived coefficients (Smith and Weintraub, 1953):

$$N = 77.6P/T + 3.73 \times 10^5 e/T^2, \tag{2}$$

where P is the atmospheric pressure (in millibars), T the absolute temperature (in degrees Kelvin), and e the water vapor pressure (in millibars). This expression consists of two terms; the first is often referred to as the dry term, and the second is often referred to as the wet term, because it is a function of water vapor. Equation (2) neglects dispersion effects and in principle does not hold near absorption lines; however, in practice it is assumed valid down to a wavelength of about 3 mm and is often considered acceptable down to wavelengths of even 1 mm, particularly in the window regions. The refractivity decreases approximately exponentially with height and is often expressed as

$$N(h) = N_s e^{-bh}, \tag{3}$$

where h is the height above sea level (in kilometers), N_s the surface refractivity, $b = 0.136$/km, and $N(h)$ is the refractivity at height h (in kilometers).

As mentioned earlier, the gross behavior of atmospheric refractivity affects millimeter waves in much the same way as microwaves; because effects such as bending, time delay, and ducting are amply treated elsewhere (Bean and Dutton, 1968), they will only be summarized here. The refractive index fine scale structure is too complex to be treated by simple refraction theory. Because of the variability in the scale sizes of the refractive inhomogeneities, the effects are wavelength dependent, and thus the interaction is different for millimeter waves than for microwaves.

a. *Bending.* The angular bending is due primarily to the change of the index of refraction of the atmosphere with height. Because the refractivity generally decreases with height, the wave passing obliquely through the atmosphere is bent downward. Thus the apparent elevation angle of a target tends to appear slightly higher than its true elevation angle, and this difference is called the angle error. For a horizontally stratified atmosphere the angle error is zero at zenith and increases very slowly with decreasing elevation angle. This error becomes appreciable at low elevation angles, and for a standard atmosphere it approaches a value of about 0.07° near the horizon. For illustration we plot in Fig. 1 the angle errors of targets at

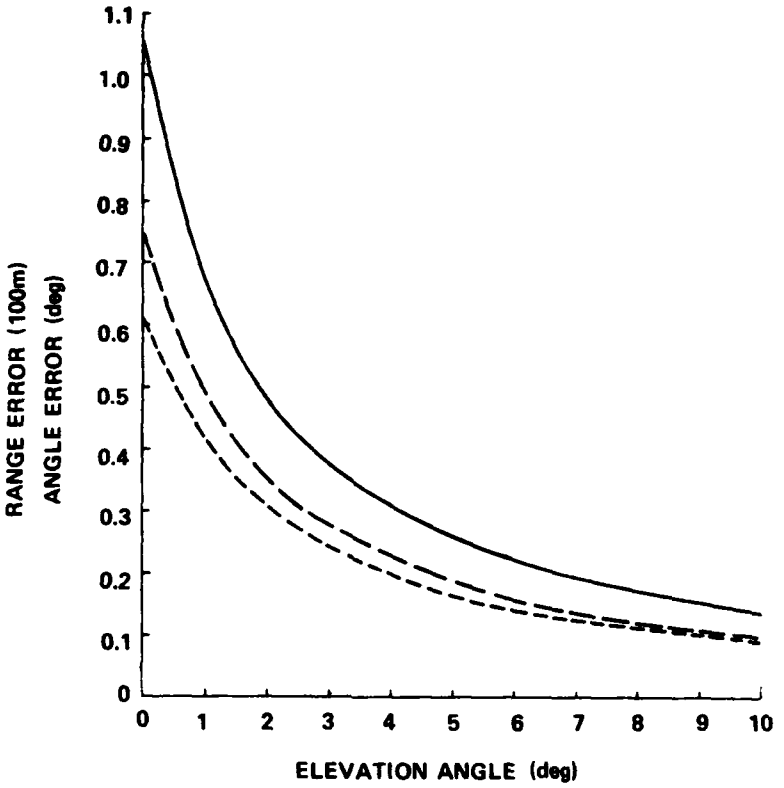

FIG. 1 Typical tropospheric refraction angle and range errors: ——, range error; — —, angle error ($h = \infty$); – – –, angle error ($h = 90$ km). CRPL reference atmosphere, 1958. (From Altshuler and Mano, 1982. Reproduced by permission of the U.S. Dept. of Commerce, National Technical Information Service, Springfield, Virginia 22161.)

altitudes of 90 km and infinity (radio source) for an atmosphere with a surface refractivity of 313 N units that decreases exponentially with height.

For a typical atmosphere the refractivity decreases at a rate of about 40 N units/km near the surface and then more slowly at higher altitudes; this produces superrefraction. As the gradient of this decrease in refractivity becomes larger the wave is bent more toward the earth's surface, and when the gradient decreases at a rate of 157 N units/km the wave travels parallel to the surface; this condition is called ducting. For still steeper gradients the wave will actually be bent into the earth. There are times when the decrease in refractivity is less than 40 N units/km and the wave is bent less than normal toward the earth; this is called subrefraction.

In actuality we have a curved ray passing over a curved earth. It is sometimes easier to visualize a straight ray over a curved earth (or a curved ray over a flat earth). For a vertical negative gradient of 40 N units/km, it can

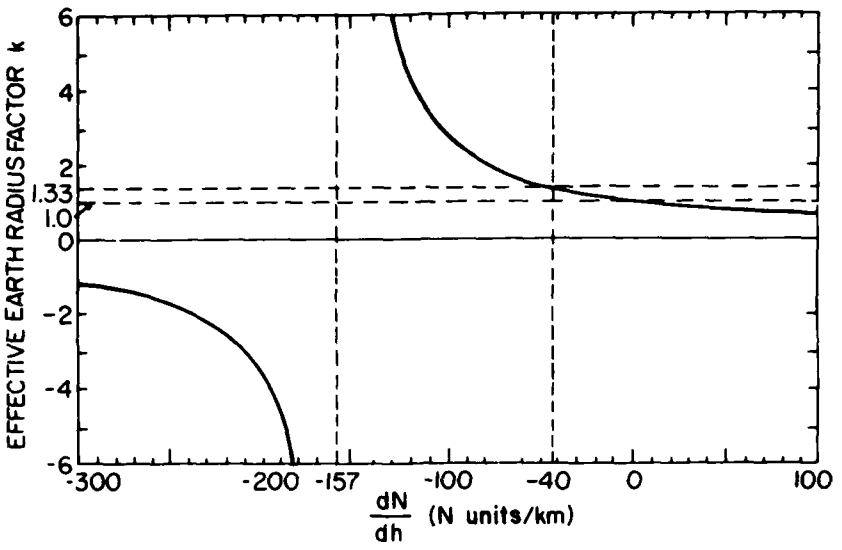

FIG. 2 Effective earth radius factor as a function of refractive index gradient dN/dh: ducting region, $dN/dh < -157$ N units/km, $K < 0$; supperrefraction region, -157 N units/km $< dN/dh < -40$ N units/km, $0 < K < \infty$; subrefraction region, -40 N units/km $< dN/dh$, $\infty < K < 0$. (From Hall, 1979. © Peter Peregrinus Ltd.)

be shown that an earth with an effective radius about $\frac{4}{3}$ that of the true earth with the wave propagating in a straight line is equivalent to the true case—the curved ray path over the curved earth. The ratio of the effective earth radius to the true earth radius is often designated k. The behavior of k as a function of the refractive index gradient is illustrated in Fig. 2 (Hall, 1979). If the refractivity gradient is less than 40 N units/km, then k decreases and reaches unity for the case of no gradient. As the gradient becomes more positive, k approaches zero. When the negative gradient is more negative than 40 N units/km, k is larger than $\frac{4}{3}$ and approaches infinity for the special case of ducting, for which the gradient reaches 157 N units/km. For still larger negative gradients, k becomes negative, because the flat earth for $k = \infty$ becomes curved in the opposite sense.

b. *Time Delay.* Time delay occurs primarily because the index of refraction of the atmosphere is greater than unity, thus slowing down the wave, and to a lesser extent because of the lengthening of the path by angular bending. For radar and navigation systems the range is determined from time delay measurements; thus the additional time delay produced by the troposphere results in a corresponding range error. This error causes the target to appear further away than its true distance. For a typical atmosphere the range error is slightly larger than 2 m in the zenith direction and

increases very slowly with decreasing elevation angle. The range error becomes much larger at lower elevation angles, and for a standard atmosphere it approaches a value of about 100 m near the horizon. For illustration, we plot in Fig. 1 the range error for an atmosphere with a surface refractivity of 313 N units that decreases exponentially with height.

c. *Refraction Corrections.* As seen in Fig. 1, the angle and range errors become appreciable for very low elevation angles. It has been shown that both errors are strongly correlated with the surface refractivity, and for many applications adequate corrections based on a linear regression on N_s are possible (Altshuler, 1970; Bean and Dutton, 1968). More accurate corrections can be obtained by measuring the vertical refractivity profile and calculating the corrections. The principal limitation of this approach is that a horizontally stratified atmosphere is usually assumed, and this is not always valid for the long distances traversed at low elevation angles. It has been shown that the range error is correlated with the brightness temperature of the atmosphere, and techniques to take advantage of this dependence have been proposed (Elgered, 1982; Gallop and Telford, 1975; Schaper *et al.*, 1970; Westwater, 1976; Wu, 1979).

One of the most effective methods for obtaining angle error corrections involves the use of "targets of opportunity." These may be either calibration satellites or radio sources, the angular positions of which are normally known to an accuracy of the order of microradians. In principle, the angular error of the calibration source is measured prior to the target being tracked. If the target is in the same general direction as the calibration source and the atmospheric refractivity does not change appreciably with time, then the correction can be determined directly. It is more difficult to use this technique to obtain range error corrections, because the true range of a satellite is generally not known to sufficient accuracy for calibration and, because radio sources are detected passively, no range information is available. However, Mano and Altshuler (1981) and Altshuler and Mano (1982) have derived an expression for the range error as a function of angle error and show that range error corrections can be obtained from a set of angle error corrections.

d. *Tropospheric Multipath.* We have seen in Section II.A.1.a that for a superrefractive troposphere the rays are bent toward the earth and that in extreme cases the waves can follow the earth's curvature (ducting). The same type of refractivity structure can also produce tropospheric multipath, in which rays are essentially reflected from layers set up by these large negative gradients in refractive index. The mechanism that produces tropospheric multipath has been modeled by Rummler (1979), who used both two- and three-ray models to show how tropospheric multipath can affect line-of-sight propagation. The model is heavily dependent on the refractive

index structure, the separation of transmitter and receiver, and the location of each with respect to the layer. Generally, the likelihood of multipath occurring increases as the separation between transmitter and receiver increases or as the transmitter and receiver come closer to the layer. Multipath effects may be lessened by employing antenna beamwidths that are narrow enough that the layer is well outside the main beam.

Experiments to study multipath propagation have been conducted by many investigators, using two different techniques. In one method a very short pulse is transmitted and the time delays between the direct signal and the multipath signals are measured. Time delays are usually of the order of nanoseconds, and the amplitudes of the delayed signals generally decrease with increasing delay. An equivalent technique makes use of a swept frequency; the delays are not measured directly but are obtained through a Fourier transform of the transfer function. Stephanson (1981) has summarized the results obtained from these experiments in a very complete review paper.

Of particular interest are the experimental results obtained by Sandberg (1980). These are in good agreement with Rummler's three-ray model, which seems to give a more complete description of the multipath phenomenon, in terms of both the time delay of the signal and its angle of arrival, than the two-ray model. The effects of tropospheric multipath on line-of-sight propagation will be discussed in more detail in Section III.A.

e. *Scintillations.* So far we have discussed the effects of the gross refractivity structure of the atmosphere on the propagated wave. The atmosphere also has a fine scale refractive index structure, which varies both temporally and spatially and thus causes the amplitude and phase of a wave to fluctuate; these fluctuations are often referred to as scintillations. The refractive index structure is envisioned to consist of pockets of refractive inhomogeneities that are sometimes referred to as turbulent eddies and may be classified by size into three regions: the input range, the inertial subrange, and the dissipation range. The two boundaries that separate these regions are the outer and inner scales of turbulence, L_0 and l_0, respectively. These are the largest and smallest distances for which the fluctuations in the index of refraction are correlated. A meteorological explanation of how these pockets are generated is beyond the scope of this book; however, in simple terms, large parcels of refractivity, possibly of the order of hundreds of meters in extent, continually break down into smaller-scale pockets. These pockets become smaller and smaller until they finally disappear. The very large pockets in the input range have a complex structure, and at the present time there is no acceptable formulation of the turbulence properties of this region. Pockets having scale sizes of less than about 1 mm have essentially

no turbulent activity, and for all practical purposes the spectrum of the covariance function of the refractive index fluctuations, $\phi_n(k)$, equals zero. The inertial subrange bounded by L_0 and l_0 has a spectrum

$$\phi_n(k) = 0.033 C_n^2 k^{-11/3} \tag{4}$$

for $2\pi/L_0 < k < 2\pi/l_0$, where C_n is the structure constant and k the wave number (not to be confused with the ratio k of the effective earth radius to the true earth radius used earlier).

The phase fluctuations arise from changes in the velocity of the wave as it passes through pockets of different refractive index. As the wavelength becomes shorter, the changes in phase increase proportionally. The amplitude fluctuations arise from defocusing and focusing by the curvature of the pockets. A detailed explanation of millimeter-wave scintillations is provided by Strobehn (1968) and Fante (1980).

2. *Absorption and Emission*

Atmospheric gases can absorb energy from millimeter waves if the molecular structure of the gas is such that the individual molecules possess electric or magnetic dipole moments. It is known from quantum theory that, at specific wavelengths, energy from the wave is transferred to the molecule, causing it to rise to a higher energy level; if the gas is in thermal equilibrium it will then reradiate this energy isotropically as a random process, thus falling back to its prior energy state. Because the incident wave has a preferred direction and the emitted energy is isotropic, the net result is a loss of energy from the wave. The emission characteristics of the atmosphere may be represented by those of a blackbody at a temperature that produces the same emission; therefore the atmospheric emission is often expressed as an apparent sky temperature. Because absorption and emission are dependent on the same general laws of thermodynamics, both are expressed in terms of the absorption coefficient. Using Kirchhoff's law and the principle of conservation of energy, one can derive the radiative transfer equation, which describes the radiation field in the atmosphere that absorbs and emits energy. This emission is expressed as

$$T_a = \int_0^\infty T(s)\gamma(s) \exp\left(-\int_0^\infty \gamma(s')\, ds'\right) ds, \tag{5}$$

where T_a is the effective antenna temperature, $T(s)$ the atmospheric temperature, $\gamma(s)$ the absorption coefficient, and s the distance from the antenna (ray path). In simpler terms

$$T_a = T_m(1 - e^{-\gamma s}), \tag{6}$$

where T_m is the atmospheric mean absorption temperature within the antenna beam. Solving for the attenuation,we obtain

$$A = \gamma s = 10 \log[T_m/(T_m - T_a)], \tag{7}$$

where A is measured in decibels. The only atmospheric gases with strong absorption lines at millimeter wavelengths are water vapor and oxygen. The absorption lines of O_3, CO, N_2O, NO_2, and CH_2O are much too weak to affect propagation in this region.

a. *Water Vapor.* The water vapor molecule has an electric dipole moment with resonances at wavelengths of 13.49, 1.64, and 0.92 mm (22.24, 183.31, and 325.5 GHz) in the millimeter-wave region. In general, the positions of these resonances, their intensities, and their linewidths agree well with experimental data. There are, however, serious discrepancies between theoretical and experimental absorption coefficients in the window regions between these strong lines; experimental attenuations are often a factor of two to three times larger than theoretical values (URSI Commission F Working Party, 1981). Although the cause of the discrepancy is not known, indications are that either the line shapes do not predict enough absorption in the wings of the resonances or there is an additional source of absorption that has not yet been identified. It should be mentioned that there are over 1800 water vapor lines in the millimeter-wave–infrared spectrum, 28 of which are above 0.3 mm. Because the wings of these lines contribute to the absorption in the window regions, very small errors in the line shapes could significantly affect the overall absorption. In an effort to overcome this problem, several workers have introduced an empirical correction term to account for the excess attenuation (Crane, 1980a; Waters, 1976).

In addition to the uncertainty of the absorption coefficient of water vapor, there is also the problem of water vapor concentration. The amount of water vapor in the lower atmosphere is highly variable in time and altitude and has densities ranging from a fraction of a gram per cubic meter for very arid climates to 30 g/m^3 for hot and humid regions; for this reason it is very difficult to model. A plot of the water vapor absorption as a function of wavelength is shown in Fig. 3 for a density of 7.5 g/m^3. Because the attenuation is linearly proportional to the water vapor density, except for very high concentrations, attenuations for other water vapor densities are easily obtained.

b. *Oxygen.* The oxygen molecule has a magnetic dipole moment with a cluster of resonances near a wavelength of 5 mm (60 GHz) and a single resonance at 2.53 mm (118.75 GHz). Although the more than 30 lines near

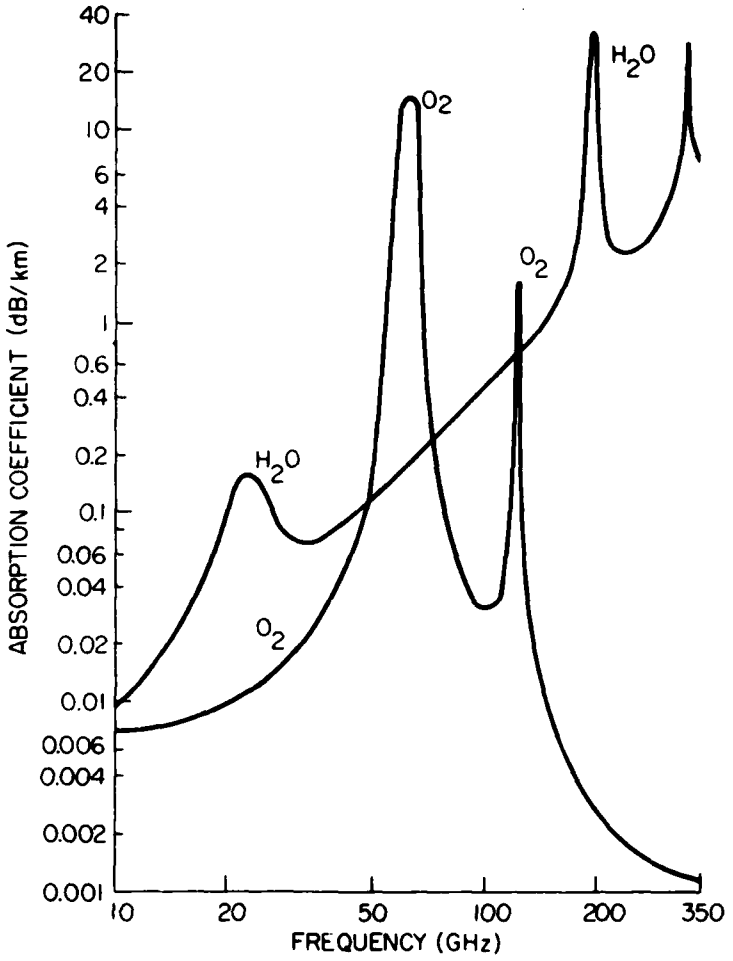

FIG. 3 Absorption coefficients for water vapor and oxygen. $P = 1$ atm, $T = 20°C$, $P_w = 7.5$ g/m^3. (From Smith, 1982. © American Geophysical Union.)

a wavelength of 5 mm are resolvable at low pressures (high altitudes), they appear as a single pressure-broadened line near sea level owing to a large number of molecular collisions. Even though the magnetic dipole moment of oxygen is approximately two orders of magnitude weaker than the electric dipole moment of water vapor, the net absorption due to oxygen is still very high, simply because it is so abundant. The fact that the distribution of oxygen throughout the atmosphere is very stable makes it easy to model. A plot of oxygen attenuation as a function of wavelength is shown in Fig. 3 along with that of water vapor. Note the importance of water vapor attenuation at very short wavelengths.

3. *Scattering*

The principal effect of the pockets of refractive index on the propagated wave is to produce scintillations, as described in Section II.A.1. When the pockets are of the order of a wavelength in size, they can also scatter the signal. At millimeter wavelengths and for line-of-sight paths, this scattered field is generally very weak compared to the direct signal and is not considered significant. There are, however, special cases for which the scattered field is important, and these are considered next.

a. *Troposcatter.* Signals propagated at angles very close to the horizon can be received at distances far beyond the horizon; this mode of propagation is called tropospheric scatter propagation, or simply troposcatter. There is still not complete agreement on the mechanism that produces the scattered field; however, two models in particular have been used through the years. Probably the most widely held view is that of scattering from turbulent pockets originally proposed by Booker and Gordon (1950). Another view is that the scattering takes place from very thin layers of refractivity (Friis *et al.*, 1957). More recently, Crane (1981) has suggested that both of these models may be valid depending on the wavelength, the scatter angle, and the thickness of the layer. By using very-high-power radars in a backscatter mode, it has been possible to observe thin turbulent layers (Crane, 1973; Hooke and Hardy, 1975). Crane believes that if the wavelength λ, scatter angle θ, and vertical outer scale of turbulence L_{0v} satisfy the condition

$$\lambda/2 \sin \tfrac{1}{2}\theta > L_{0v}, \tag{8}$$

then the layer model is valid and the mechanism is predominantly one of partial specular reflection from the layer. This model applies best for longer wavelengths. When Eq. (8) is not satisfied, the mechanism is believed to be predominantly volume scattering from the pockets that compose the layer. Because the outer scale of turbulence and scattering angle are typically of the order of kilometers and 1°, respectively, it is seen from Eq. (8) that troposcatter at millimeter wavelengths is indeed volume scattering from turbulent pockets. Most turbulence theories assume a Kolmogorov energy spectrum with a wavelength dependence of $\lambda^{5/3}$. This in turn leads to a scattering cross section per unit volume proportional to $\lambda^{1/3}$. The elevation angle dependence is proportional to $\theta^{11/3}$. Although the scattered signal and antenna gain increase with decreasing wavelength, this increase is limited by the aperture-to-medium coupling loss and atmospheric attenuation. These limitations will be reviewed in Section III.C.

b. *Terrain Multipath.* Electromagnetic waves scattered from the earth's surface may interfere with the direct signal; this is called multipath

propagation. The extent of multipath is dependent on the geometry of the transmitter and receiver with respect to the surface, their respective beamwidths and polarizations, and the dielectric constant and surface roughness of the terrain.

Let us first consider a surface that is relatively smooth with respect to wavelength. The reflection coefficients of vertically and horizontally polarized waves for a nonmagnetic surface are

$$\Gamma_v = \frac{\varepsilon \sin \alpha - (\varepsilon - \cos^2 \alpha)^{1/2}}{\varepsilon \sin \alpha + (\varepsilon - \cos^2 \alpha)^{1/2}}, \tag{9}$$

$$\Gamma_h = \frac{\sin \alpha - (\varepsilon - \cos^2 \alpha)^{1/2}}{\sin \alpha + (\varepsilon - \cos^2 \alpha)^{1/2}}, \tag{10}$$

where α is the grazing angle and $\varepsilon = \varepsilon' - j\varepsilon''$ the complex dielectric constant. Typical values of the magnitudes and phases of these reflection coefficients as a function of grazing angle are shown in Figs. 4 and 5 (Povejsil *et al.*, 1961). For very small grazing angles the magnitudes approach unity and the phases approach 180°. As the grazing angle increases, the magnitude and phase of the vertically polarized wave fell off sharply and those of the horizontally polarized wave decrease very slightly. The sharp falloff of the

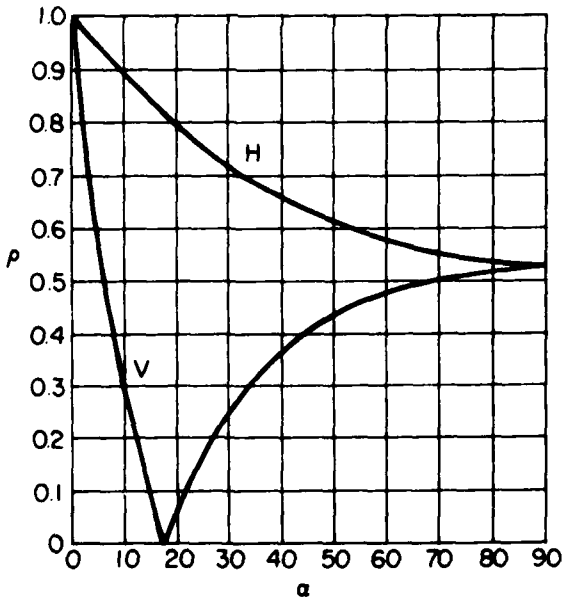

FIG. 4 Magnitude of reflection coefficient ρ for average land as a function of incidence angle α ($\varepsilon' = 10$, $\sigma = 1.6 \times 10^{-3}$ S/m). (From "Airborne Radar" by Donald J. Povejsil, Robert S. Raven, and Peter Waterman. © 1961 by D. Van Norstrand Company, Inc. Reprinted by permission of Wadsworth Publishing Company, Belmont, California 94002.)

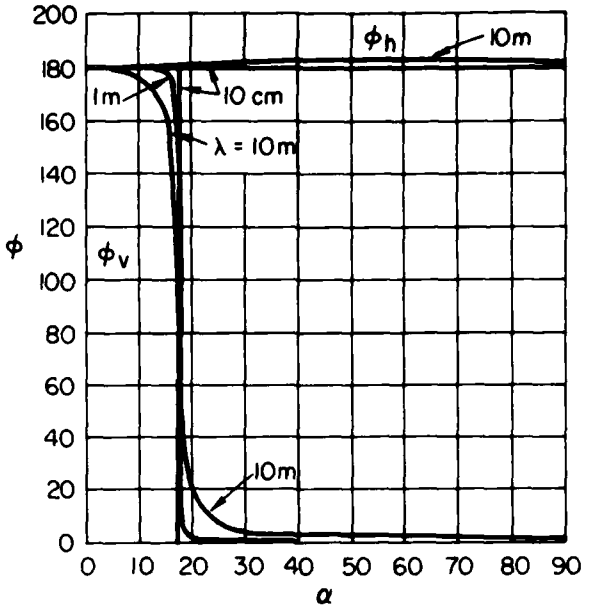

FIG. 5 Phase ϕ of reflection coefficient for average land as a function of incidence angle α ($\varepsilon' = 10$, $\sigma = 1.6 \times 10^{-3}$ S/m). (From "Airborne Radar" by Donald J. Povejsil, Robert S. Raven, and Peter Waterman. © 1961 by D. Van Norstrand Company, Inc. Reprinted by permission of Wadsworth Publishing Company, Belmont, California 94002.)

vertically polarized reflection coefficient can be explained as follows. For most surfaces, with the exception of very dry ground, $|\varepsilon| \gg 1$. With this approximation, Eq. (9) can be rewritten as

$$\Gamma_v = (\sqrt{\varepsilon} \sin \alpha - 1)/(\sqrt{\varepsilon} \sin \alpha + 1). \tag{11}$$

Note that the numerator is $\sqrt{\varepsilon} \sin \alpha - 1$. Thus at some angle the numerator approaches zero; this is the Brewster angle, and if the terrain were a perfect dielectric ($\sqrt{\varepsilon}$ is real) then the reflection coefficient would actually go to zero. As the grazing angle approaches normal incidence the vertical reflection coefficient increases and finally equals the horizontally polarized reflection coefficient at normal incidence.

When the surface is relatively smooth the scattering is predominantly specular; that is, it can be considered coherent. As the surface becomes rougher a diffuse, incoherent component appears, and for a very rough surface the scattered signal is predominantly diffuse. The criterion usually applied for characterizing surface roughness is that introduced by Rayleigh. It is based on the phase difference of adjacent rays reflected from a rough surface; when the path difference between these rays increases to 90°, the surface is assumed to transform from smooth to rough. Obviously this

transition is very gradual and should be interpreted as such. Mathematically the surface can be considered smooth when $h \sin \alpha < \frac{1}{8}\lambda$, where h is the height of a surface irregularity. It must be emphasized that even at millimeter wavelengths, for which λ is very small, typical surfaces tend to look smooth at very low grazing angles.

We have reviewed the general characteristics of multipath propagation. Now let us summarize multipath propagation in the context of millimeter waves. At longer wavelengths the reflection coefficient of a vertically polarized wave is significantly lower than that of a horizontally polarized wave, particularly in the vicinity of the Brewster angle, so microwave systems are often designed to operate with vertical polarization to minimize multipath interference. At millimeter wavelengths this polarization dependence is of less importance, because the reflection coefficients of vertically and horizontally polarized waves are comparable for most millimeter-wave applications. First of all, multipath effects at these short wavelengths will generally occur only at very small grazing angles, because most surfaces based on the Rayleigh criterion appear rough for larger grazing angles. Furthermore, because the dielectric constants of most surfaces tend to remain constant or decrease with decreasing wavelength, the Brewster angle increases and the reflection coefficient of the vertically polarized wave does not drop off as rapidly with increasing grazing angle. Therefore at millimeter wavelengths multipath is confined to much lower grazing angles than at microwave wavelengths and is thus less sensitive to polarization. In Fig. 6, Rayleigh's roughness criterion is plotted as a function of grazing angle. As the surface becomes rough with respect to wavelength, the grazing angle must become extremely small to have specular reflection.

4. *Diffraction*

Electromagnetic waves incident on an obstacle may be bent around that obstacle; this is known as diffraction. The extent of diffraction is dependent on the shape and composition of the obstacle, its position with respect to the direct path of the incident wave, and the wavelength. Classical diffraction theory has been used to treat simple shapes such as individual knife edges, rounded edges, and in some instances sets of these edges. An underlying assumption is that the knife edge is very sharp or the rounded edge very smooth with respect to wavelength. It is also often assumed that the edge is a perfect conductor, although solutions have been obtained for edges having finite conductivity.

Diffraction loss is often expressed as a function of the dimensionless Fresnel parameter v, which is in turn a function of the geometric parameters of the obstacle and path. For knife edge diffraction the Fresnel parameter can be defined as

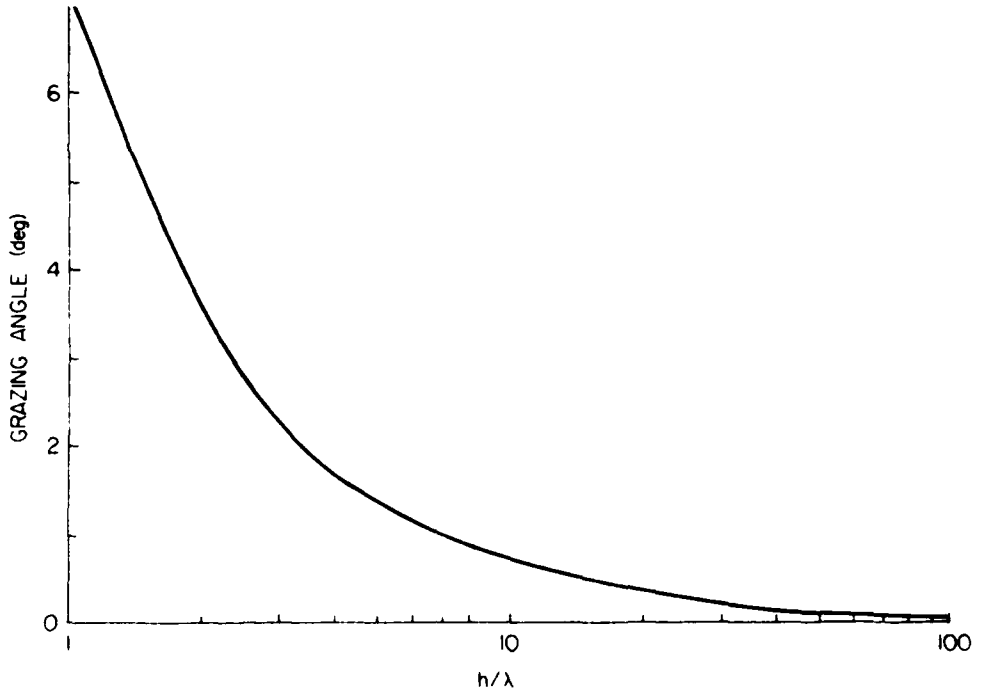

FIG. 6 Rayleigh roughness criterion.

$$v = h\left[\frac{2}{\lambda}\left(\frac{1}{d_1}+\frac{1}{d_2}\right)\right]^{1/2}, \tag{12}$$

where h is either the height of the obstacle above the direct path or the distance of the obstacle below the path, and d_1 and d_2 are the respective distances of transmitter and receiver from the knife edge. For illustration, let us assume that the knife edge is midway between transmitter and receiver; then $d_1 = d_2 = \frac{1}{2}d$ and

$$|v|^2 = 8h^2/\lambda d, \tag{13}$$

where v is positive when the ray path is below the edge and negative when the ray path is above the edge. It is known that the diffraction loss is approximately zero for $v < -3$ and very high for $v > 3$, so $-3 \le v \le 3$ can be considered the region of interest.

Equation (13) can be expressed as

$$h = \sqrt{\tfrac{1}{8}\lambda d v^2} = \tfrac{1}{2}v\sqrt{\tfrac{1}{2}\lambda d}. \tag{14}$$

Because d is generally on the order of kilometers and λ on the order of millimeters, h can only be on the order of meters. Thus from a practical

standpoint only isolated obstacles such as small hills or buildings would produce diffraction effects at millimeter wavelengths.

5. *Depolarization*

Depolarization of an electromagnetic wave can occur when the incident wave is scattered and a cross-polarized component is produced along with the copolarized component. It is defined as

$$|\text{depolarization}| = 20 \log(|E_x|/|E_y|), \tag{15}$$

where E_x and E_y are the cross-polarized and copolarized components, respectively, and the depolarization is measured in decibels. Olsen (1981) has summarized in detail both the mechanisms that can produce depolarization during clear air conditions and some experimental observations of this phenomenon. He divides these mechanisms into two groups: those that are independent of the cross-polarized pattern of the antenna (a perfect plane-polarized wave) and those that are dependent on the cross-polarized pattern. In principle, depolarization can arise from scattering by refractive inhomogeneities or from terrain. For the plane-polarized wave it appears that depolarization due to refractive multipath is insignificant (Olsen, 1981) but that depolarization due to terrain multipath can be much stronger. For an antenna having a measurable cross-polarized pattern, it is believed that both atmospheric and terrain multipath mechanisms contribute to the depolarization of the wave. Although most experimental results of depolarization by the clear atmosphere have been obtained at centimeter wavelengths, there is no reason to believe that the same effects will not occur at millimeter wavelengths. However, because both atmospheric and terrain multipath may normally be weaker at millimeter wavelengths than at microwave wavelengths, the depolarization may not be as severe.

B. Atmospheric Particulate Effects

In this section we discuss the degrees of absorption, scattering, and depolarization that may occur from atmospheric particulates. We shall see that rain is by far the most important of the particulates, for two reasons: the interaction of rain with millimeter waves is very strong and rain occurs more often than other particulates. Thus a detailed discussion of the rain–millimeter-wave interaction is presented.

1. *Absorption and Scattering*

Millimeter waves incident on atmospheric particulates undergo absorption and scattering, the degree of each being dependent on the size, shape, and complex dielectric constant of the particle and the wavelength and

polarization of the wave. An expression for calculating the absorption and scattering from a dielectric sphere was first derived by Mie (1908):

$$Q_t = -\lambda^2/2\pi \operatorname{Re} \sum_{n=1}^{\infty} (2n+1)(a_n^s + b_n^s), \tag{16}$$

where Q_t represents losses due to both absorption and scattering, and a_n^s and b_n^s are very complicated spherical Bessel functions that correspond to the magnetic and electric modes of the particle, respectively. Q_t has the dimension of area and is usually expressed in square centimeters. Physically, if a wave with a flux density of S W/cm^2 is incident on the particle, then $\mathbf{S} \times \mathbf{Q}_t$ is the power absorbed or scattered.

When the circumference of the particle is very small compared to wavelength, i.d., $\pi D \ll \lambda$, then the scattering and absorption losses can be represented by

$$Q_s = (\lambda^2/2\pi)(\tfrac{4}{3}\rho^6)|(n^2-1)/(n^2+2)|^2 \tag{17}$$

and

$$Q_a = (\lambda^2/2\pi)(2\rho^3) \operatorname{Im}[-(n^2-1)/(n^2+2)], \tag{18}$$

where $\rho = kD/2 = \pi D/\lambda \ll 1$ and n is the complex index of refraction.

Because ρ is very small, the loss due to scattering, which is proportional to ρ^6, will be much smaller than that due to absorption, which is proportional to ρ^3. This condition is often referred to as the Rayleigh approximation, for which

$$Q_s \propto 1/\lambda^4 \qquad \text{and} \qquad Q_a \propto 1/\lambda.$$

Because the scattering loss is often assumed negligible, the total loss is proportional to the volume of the drop. Often the backscatter cross section (or radar cross section) is of interest:

$$\sigma = (\lambda^2\rho^6/\pi)|(n^2-1)/(n^2+2)|^2 = \tfrac{1}{2}Q_s. \tag{19}$$

The relationship with Q_s arises because Rayleigh scatterers are assumed to have the directional properties of a short dipole and the directivity of a dipole in the backscatter direction is 1.5 times that of an isotropic source. As the drop becomes large with respect to wavelength, the Rayleigh approximation becomes less valid and the Mie formulation must be used.

2. *Depolarization*

Atmospheric particulates having a nonspherical shape will depolarize a wave (produce a cross-polarized component) if the major or minor axis of the particulate is not aligned with the E-field of the incident wave. The extent of the depolarization is a strong function of the size, shape, orienta-

tion, and dielectric constant of the scatterer. The depolarization defined in Eq. (15) arises because the orthogonal components of the scattered field undergo different attenuations and phase shifts. These differences are referred to as the differential attenuation and differential phase shift. An alternative definition related to depolarization is the cross-polarization discrimination, which is simply the reciprocal of the depolarization. In general, the depolarization increases as the particulate size and eccentricity increase. The depolarization also increases as the angle between the E-field of the incident wave and the major axis of the particulate increases up to approximately 45°, for which the depolarization passes through a maximum.

3. *Types of Particulates*

Rain is the most common particulate; drops range in size from a fraction of a millimeter to 6 or 7 mm. Sleet and snow, which are considered quasi-solid forms of water, are then treated. Because of their complexity of shape and composition only limited theoretical work has been done on them, and because they are rare events in most locations only limited experimental data have been obtained. Hail is frozen water, and does not occur very often. However, the losses due to hail can be calculated quite accurately, and are very small at millimeter waves because the complex dielectric constant of ice is small. Cloud, fog, and haze particulates are very similar in that they are all composed of very small water droplets suspended in air (clouds may also contain ice crystals) with diameters ranging from several microns up to about 100 μ. Therefore, through most of the millimeter-wave region the Rayleigh approximation is valid for these particulates. Dust and sand particulates have size distributions comparable to that of clouds, but because their complex dielectric constants are low their interaction with millimeter waves is very weak.

a. *Rain.* Rain is an extremely complex phenomenon, both meteorologically and electromagnetically. From a meteorological standpoint it is generally nonuniform in shape, size, orientation, temperature, and distribution, thus making it very difficult to model. Electromagnetically, the absorption, scattering, and depolarization characteristics can be calculated only for very simple shapes and distributions. However, theoretical results do provide a qualitative understanding of the effects of rain on millimeter waves, and when they are combined with experimental data, empirical parameters can be derived and more quantitative results are possible.

Let us first examine the absorption and scattering characteristics of a single spherical raindrop. From Eq. (16) we can calculate the total cross section Q_t, which is the sum of the absorption cross section Q_a and the

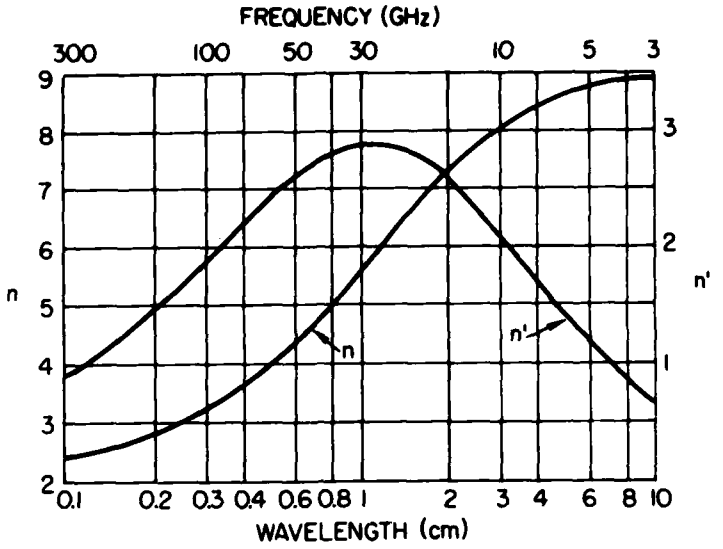

FIG. 7 Typical values of refraction indices of water at 20°C. (From Hogg and Chu, 1975. © 1975 IEEE.)

scattering cross section Q_s. This cross section is a strong function of the drop diameter and its complex index of refraction; the real and imaginary parts of the index of refraction of water are shown in Fig. 7. At millimeter wavelengths both parts decrease with decreasing wavelength, and we shall see that this is one of the reasons why the cross section of a drop eventually starts to decrease at shorter wavelengths.

In Fig. 8, the total cross section of a drop is plotted as a function of drop diameter for several wavelengths. When the drop is very small with respect to wavelength, the Rayleigh approximation is valid; it is seen from Eqs. (17) and (18) that the scattering and absorption cross sections Q_s and Q_a are proportional to $(D/\lambda)^6$ and $(D/\lambda)^3$, respectively. Because the loss due to scattering is negligible compared to that due to absorption, the total cross section is proportional to the volume of the drop. As the drop becomes larger both the scattering and absorption cross sections continue to increase, with the scattering cross section increasing more rapidly. Finally, after reaching a peak, the total cross section begins to level off, and would eventually approach a value of twice the geometric cross section of the drop when it is very large with respect to wavelength (Van de Hulst, 1957). Thus, as the drop becomes larger, the cross section, which is initially proportional to the drop volume, becomes proportional to the drop area.

The dependence of the cross section on wavelength is more complicated than that of size, because both the relative drop size and the complex index of refraction are changing. In Fig. 9, the cross sections are plotted as a

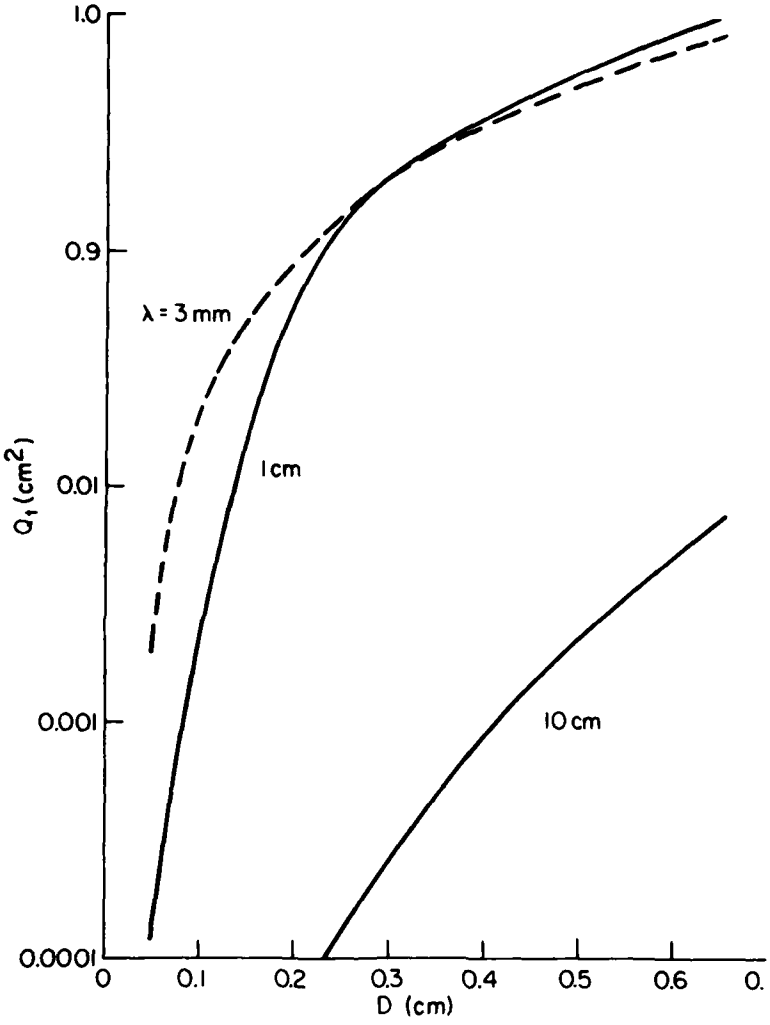

FIG. 8 Total cross section Q_t of a raindrop as a function of drop diameter D.

function of wavelength for a number of drop sizes. The cross sections increase with decreasing wavelength, reach a peak, and then start to decrease very slightly for still smaller wavelengths. This behavior can be explained by referring to Figs. 7 and 8. Although the cross section increases as the drop becomes larger with respect to wavelength, the real and imaginary components of the index of refraction decrease as the wavelength becomes smaller, and this decrease eventually causes the total cross section to decrease.

We shall now consider the effect of the *shape* of rain drops on electromagnetic parameters. Whereas small drops tend to be spherical in shape, larger drops become oblate because of distortion due to air drag and are often

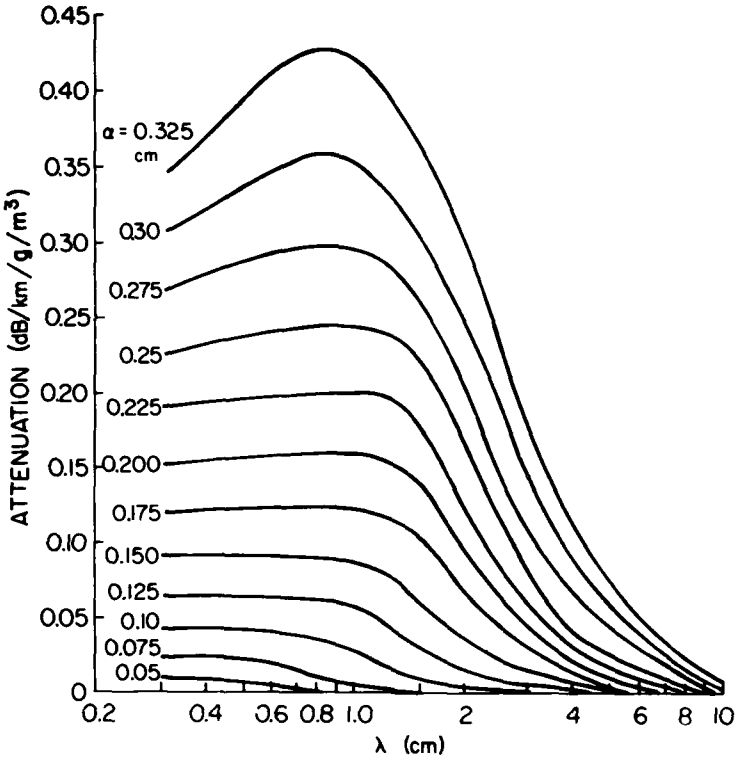

FIG. 9 Theoretical values of attenuation by raindrops for various drop radii, expressed in decibels per kilometer per drop per cubic meter. (From "Propagation of Short Radio Waves" by D. E. Kerr. © 1951, McGraw-Hill Book Company.)

modeled as oblate spheroids (Pruppacher and Pitter, 1971). The cross section of an oblate drop is generally larger than that of a corresponding spherical drop having an equal volume of water (Atlas *et al.*, 1953). The cross section is strongly dependent on the polarization of the wave, being larger when the polarization vector is aligned with the major axis of the spheroid and smaller when the polarization vector is aligned with the minor axis. We shall see that the most significant effect of a nonspherical drop is the depolarization it can produce.

We have reviewed the absorption and scattering characteristics of individual raindrops and found that they are a very complex function of both the drop geometry and the index of refraction. Rain can be considered a collection of drops having diameters ranging from a fraction of a millimeter (mist) up to possibly 7 mm. To compute the attenuation of rain the cross sections of the drops must be calculated and then summed. Because the characteristics of a precipitation system are controlled largely by the air flow, the net result is a collection of drops that is continually varying both spatially

and temporally; it is thus very difficult to model. It has been found that the meteorological parameter that is most easily measured and also most effectively characterizes rain is the rain rate. A number of investigators have shown that rain rate is correlated with drop size distribution; their results are summarized by Olsen *et al.* (1978). The attenuation can be expressed in the form

$$A = 0.4343 \int_0^\infty N(D) Q_t(D, \lambda)\, dD, \tag{20}$$

where $N(D)\, dD$ is the number of drops per cubic meter having diameters in the range dD, Q_t is the total cross section of each drop, and the attenuation is measured in decibels per kilometer. Rain is often assumed to have an exponential distribution of drop diameters, so that

$$N(D) = N_0 e^{-\Lambda D}, \tag{21}$$

where N_0 are Λ are empirical constants that are a function of the type of rain and more particularly the rain rate. The original rain attenuation calculations were done by Ryde and Ryde (1945); these were later refined by Medhurst (1965). Attenuations based on Medhurst's calculations are plotted as a function of rain rate in Fig. 10. These curves can be approximated by the expression

$$A = aR^b, \tag{22}$$

where a and b are numerical constants that are a function of wavelength and type of rain, R is the rain rate in millimeters per hour, and the attenuation is measured in decibels per kilometer. Olsen *et al.* (1978) calculated rain attenuation as a function of rain rate using the Mie formulation and then performed a logarithmic regression to obtain values for a and b. These values have been tabulated for frequencies from 1 to 1000 GHz, and although they are believed to provide a good approximation to the attenuation, it should be remembered that they are statistical and must be interpreted accordingly.

The depolarization characteristics of rain are very heavily dependent on the shape and orientation of the drops. Because light rain consists mostly of small drops and small drops tend to be spherical, depolarization effects are minimal. As the rain becomes heavier, the average drop size increases and the larger drops tend to become more oblate. The more oblate the drop, the larger the differential attenuation and phase between the orthogonal fields. However, it should be emphasized that these differentials do not in themselves produce depolarization; the incident field must also be tilted with respect to the axes of the drop. Because large oblates are easily canted by winds, their axes are not usually aligned with either horizontally or vertically

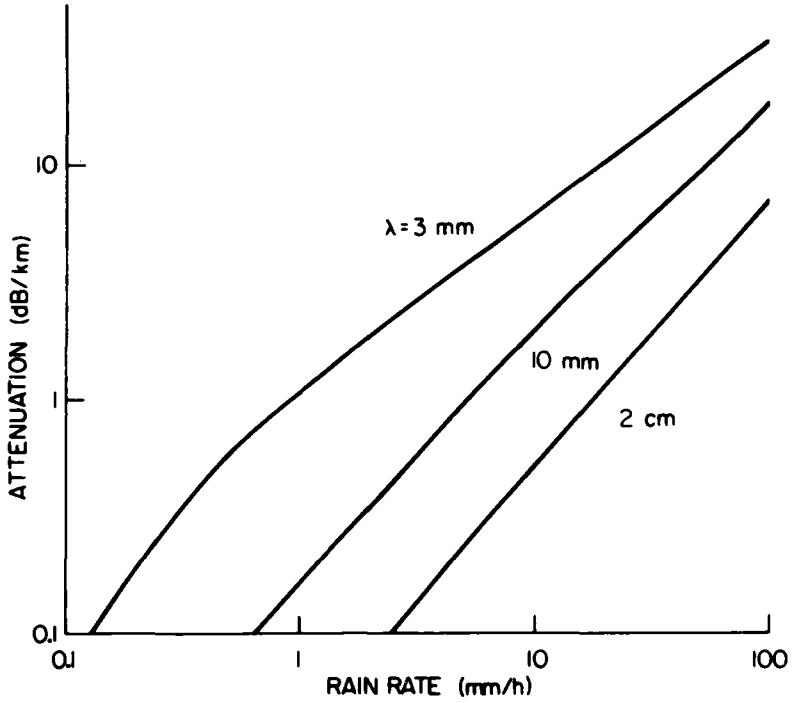

FIG. 10 Rain attenuation as a function of rain rate. (From Medhurst, 1965. © 1965 IEEE.)

polarized waves. Brussard (1976) has shown that the canting angle of oblate rain drops is a function of the average drop diameter and vertical wind gradients. Typically the canting increases with drop size and levels off for drops on the order of a few millimeters in diameter. It naturally increases with wind speed and usually becomes smaller with increasing height.

Representative curves of differential attenuations and phases of rain as a function of frequency for a number of rain rates have been prepared by Hogg and Chu (1975); these are presented in Figs. 11 and 12. Because the differential attenuation is proportional to the total attenuation, it increases with rain rate. It also initially increases with shorter wavelengths, as does the total attenuation, but then reaches a peak and eventually starts to decrease at very short millimeter wavelengths, mostly because the attenuation at very short wavelengths is produced primarily by the smaller drops and these tend to be spherical. The differential phase is affected mostly by the real part of the refractive index of water and is seen to decrease with shorter millimeter wavelengths. Thus, at millimeter wavelengths, differential attenuation is the dominant cause of depolarization.

b. *Sleet, Snow, and Hail.* These very complex forms of precipitation have attenuation characteristics that vary markedly at millimeter wave-

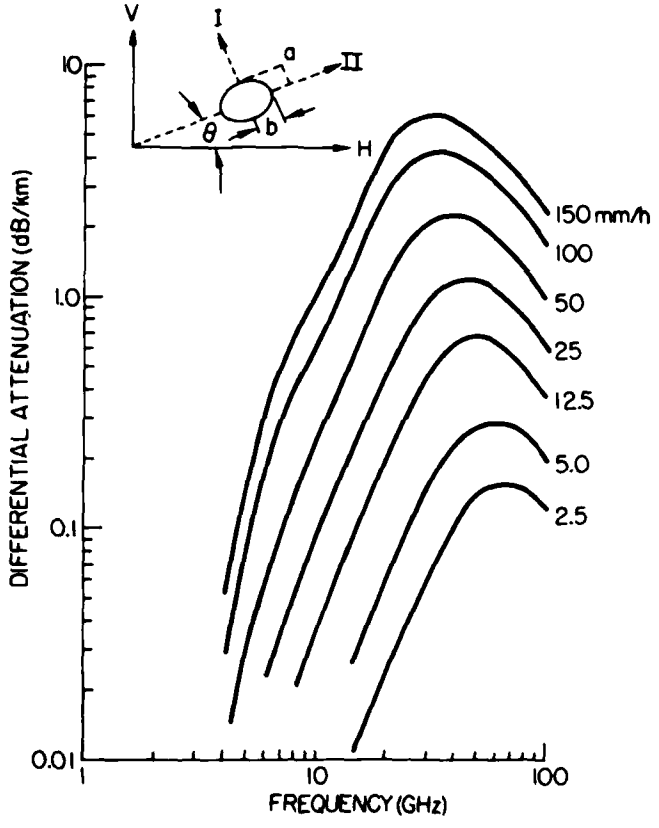

FIG. 11 Rain-induced differential attenuation. (From Hogg and Chu, 1975. © 1975 IEEE.)

lengths. We have seen that liquid water is a strong attenuator of millimeter waves; therefore sleet, which is a mixture of rain and snow, can also produce very high attenuations. In fact, these attenuations may exceed those of rain, because nonspherical shapes have been shown to produce higher attenuations than equivalent spheres and sleet particulates are often very elongated (Atlas *et al.*, 1953). The depolarization effects of sleet can be very strong if the flakes show a nonparallel preferential alignment with the *E*-field. Wet snow has characteristics very similar to those of sleet. As the snow becomes drier its composition approaches that of ice crystals, and because ice has a low imaginary index of refraction the absorption is very small. Losses due to scattering are small at longer millimeter wavelengths but may become appreciable at shorter wavelengths if the flakes are large.

The effect of hail on millimeter waves is better understood than that of sleet or snow because there is less variability in its shape and composition. Because the imaginary part of the index of refraction of ice is about three orders of magnitude less than that of water, absorptive losses are negligible.

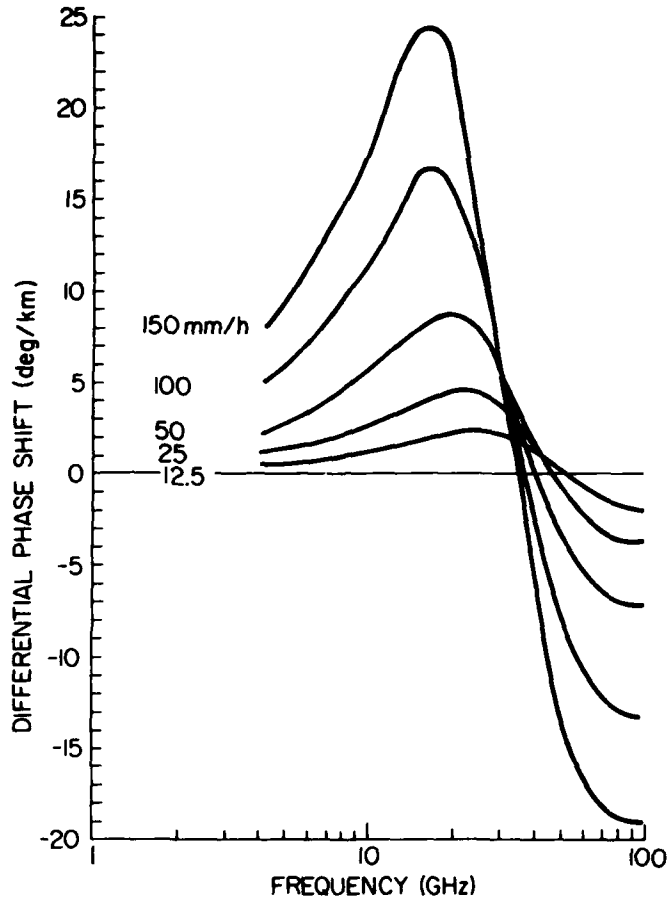

FIG. 12 Rain-induced differential phase shift. (From Hogg and Chu, 1975. © 1975 IEEE.)

The real part of the index of refraction is about one-fourth that of rain, so although scattering losses produced by hail are smaller than those of rain, they can be important, particularly at shorter millimeter wavelengths. If the hailstone is covered with even a very thin coat of water, its attenuation rises significantly and approaches that of a rain drop having an equivalent volume (Battan, 1973).

In summation, because it is extremely difficult to produce accurate models of sleet, snow, and hail, and because there are very few experimental attenuation data at millimeter wavelengths (or any other wavelengths), it is not possible to provide quantitative results. Although it is known that the absorption and scattering losses of sleet and wet snow are large and the scattering losses of dry snow and hail are significant, there are not presently any attenuation data for these particulates comparable to those for rain. However, from a practical standpoint, these particulates do not occur very

often, and so their impact on millimeter-wave systems is not considered critical.

c. *Cloud, Fog, and Haze.* Meteorologically, cloud, fog, and haze are very similar because they consist of small water droplets suspended in air. The droplets have diameters ranging from a fraction of a micron for fog and haze to over a 100 μ for heavy fog and high-altitude clouds (Stewart, 1980). Haze may be considered a light fog, and of course the principal difference between cloud and fog is that clouds exist at higher altitudes and often contain ice as well as water particulates. Electromagnetically, cloud, fog, and haze can be treated identically. Because the droplets are very small with respect to wavelength, the Rayleigh approximation is valid, even at short millimeter wavelengths. Therefore, scattering losses are negligible and the attenuation, which is proportional to the volume of the drops, can be calculated from Eq. (18) and is seen to increase with decreasing wavelength. Because it is very difficult to measure fog or cloud water content, the attenuations produced by these particulates are not easily determined. Typical attenuations are plotted as a function of wavelength in Fig. 13 for several temperatures.

Fog is often characterized by visibility, which is much easier to measure than density; however, it should be emphasized that visibility is an optical parameter, a function of the scattering characteristics of the droplets, whereas the attenuation at millimeter wavelengths, as mentioned previously, is strictly a function of the fog density. Although there is a correlation between fog or cloud visibility and total liquid water content (Eldridge, 1966; Platt, 1970), this relationship must be used with caution because the correlation coefficient is strongly dependent on the type of fog. Fog is often

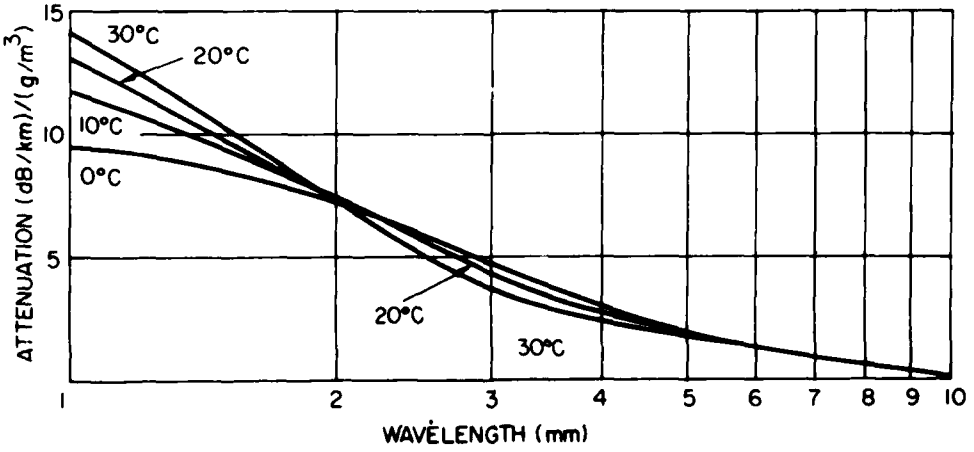

FIG. 13 Attenuation of cloud and fog as a function of wavelength.

divided into two types: radiation fog, which forms when the ground becomes cold at night and cools the adjacent air mass until it becomes supersaturated, and advection fog, which forms when warm, moist air moves across a cooler surface. The average drop size of an advection fog is usually larger than that of a radiation fog. Thus, if two fogs had the same liquid water densities but one consisted of relatively large drops, then that fog would have a much higher visibility. Another fog or cloud parameter not to be overlooked is temperature, because it has a strong influence on the complex index of refraction, particularly at longer millimeter wavelengths (Rozenberg, 1972). Once again, as with snow and hail, the overall effects of cloud and fog are not as severe as those of rain.

d. *Sand and Dust.* Sand and dust are both fine-grained, quartz-type particles that have diameters of a fraction of a millimeter, densities on the order of 2600 kg/m^3, and a relative dielectric constant of about $2.5 - 0.025i$ (Chu, 1979; Rafuse, 1981). The principal difference between sand and dust is that the average grain size of sand is larger. As a result, whereas larger wind-blown sand grains rise to a maximum height of only 2 m, heavy winds can carry fine dust particles to altitudes as high as 1 km. In general, the height to which the particles rise is proportional to the wind speed and inversely proportional to the particle size (Rafuse, 1981). Because sand and dust particulates are very small with respect to wavelength, even at millimeter wavelengths, scattering losses are negligible and the only losses are due to absorption. However, the imaginary part of the complex dielectric constant is very small; thus absorption losses can be considered minimal under naturally disturbed conditions. If a large amount of dirt or dust were to become suspended in the atmosphere as a result of an explosion, however, then significant attenuations might arise, particularly if the dust were moistened by the presence of water; these attenuations would last only for a duration of seconds (Gallagher *et al.*, 1980).

III. Transmission Paths

There are essentially three types of transmission paths, each with specific characteristics with regard to millimeter-wave propagation. Two of these paths are line-of-sight: terrestrial and earth–space. The third is the transhorizon path. We shall now take the results of Section II and apply them to systems that would use these propagation paths.

A. Terrestrial Line-of-Sight Paths

For terrestrial paths the atmospheric effects on propagation become more pronounced as the length of the path increases and the wavelength de-

creases. For short paths, attenuation is of principal concern; refraction and atmospheric multipath effects are unlikely, terrain multipath and diffraction problems arise only when transmitter and receiver are close to the surface, and depolarization and scintillations occur only under very extreme conditions of precipitation. For a clear atmosphere, gaseous absorption in the window regions is only a fraction of a decibel per kilometer at longer millimeter wavelengths but can become appreciable at shorter wavelengths. Sand and dust attenuations throughout the millimeter-wave spectrum are well below 1 dB/km, except for conditions of a large cloud that may be produced by an explosion. Haze and fog attenuations increase with decreasing wavelength as shown in Fig. 13, and although they become appreciable they are generally lower than water vapor absorption at very short wavelengths. Attenuation due to rain, sleet, and wet snow can be significant even for very short paths; this attenuation is lowest at longer wavelengths and gradually increases with decreasing wavelength, reaching a maximum at a wavelength of a few millimeters and then leveling off at still shorter wavelengths.

As the path becomes longer, attenuation effects become more severe; in addition, all of the other propagation effects mentioned in the previous paragraph are more likely to occur. The use of millimeter waves for applications requiring long terrestrial paths appears unlikely at this time because the attenuation would be prohibitive, except perhaps for a region having a relatively dry climate.

1. *Attenuation*

For many applications, particularly communications, it is important to be able to estimate the percentage of time that the path attenuation exceeds a certain value. To accomplish this one must first examine the climate of the region of interest. If the absolute humidity is known, the gaseous absorption can be estimated from the expression (CCIR, 1982a)

$$A = a + b\rho_0 - cT_0. \tag{23}$$

The coefficients are plotted in Fig. 14; ρ_0 is in grams per cubic meter and T_0 in degrees Celsius. This calculation is not very accurate at very short wavelengths, where there is a lack of agreement between the theoretical and experimental values of water vapor absorption. As mentioned in the previous paragraph, sand, dust, haze, and fog attenuations are low at longer wavelengths and generally small compared to water vapor absorption at very short wavelengths; only at wavelengths between about 2 and 3 mm is fog attenuation generally important.

Rain attenuation is by far the most serious propagation problem. Only for a few locations are rain attenuation statistics available. A procedure for

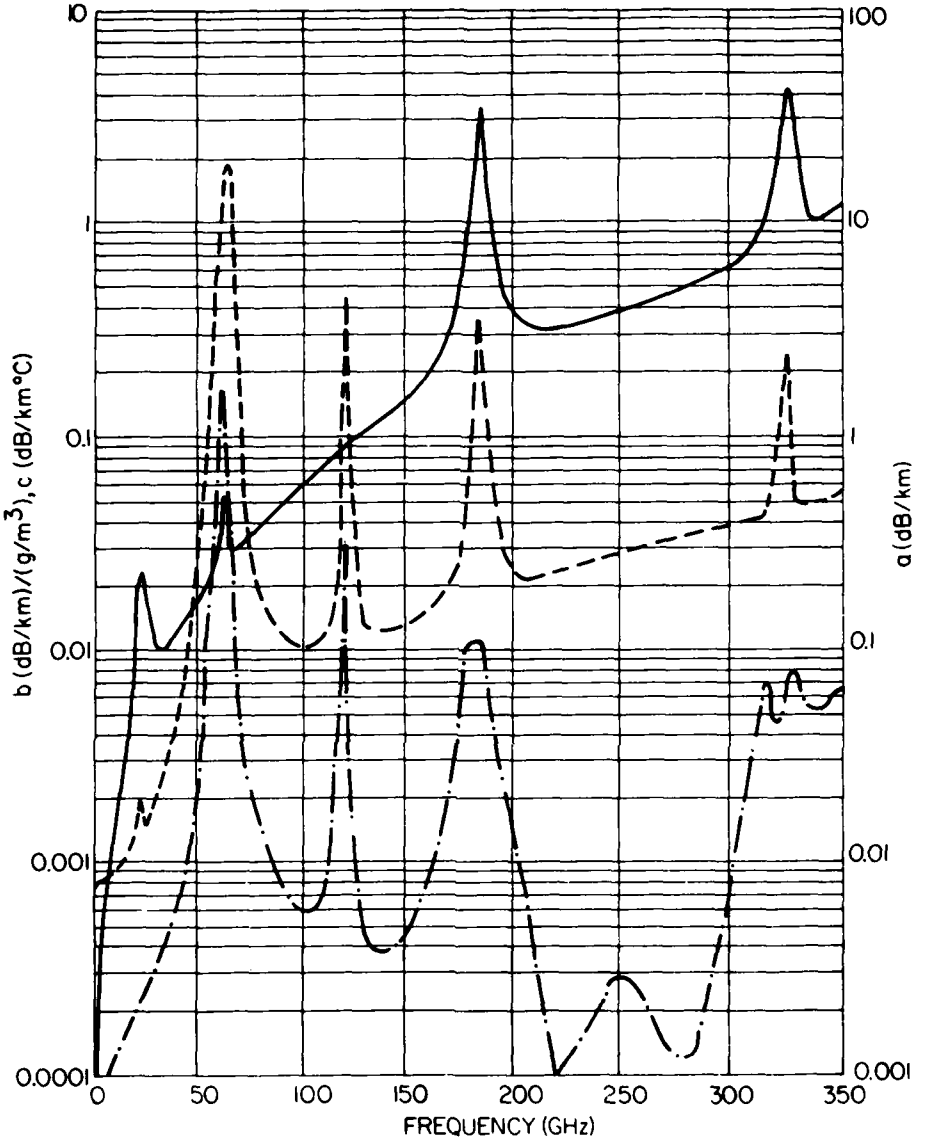

FIG. 14 Coefficients for computing specific attenuation. Specific attenuation $A = a + b\rho_0 - cT_0$ (dB/km), with ρ_0 in grams per cubic meter and T_0 in degrees Celsius: ---, a coefficient; ——, b coefficient; — · —, c coefficient. (From CCIR, 1982a).

estimating rain attenuation for different climates has been outlined by Crane (1980b). A global model representing typical rain climates throughout the world was developed, based on rain data provided by the World Meteorological Organization, and from this model the percentage of time that the point rain rate exceeds a particular value can be estimated. However, rain ordinarily consists of cells of different sizes and generally is not

homogeneous in the horizontal plane. Thus, it is necessary to derive a path average rain rate from the point values. By pooling worldwide rain statistics it was possible to obtain an empirical relationship between point and path average rain rates; this has been done so far for distances up to 22.5 km. For low rain rates the rain is usually widespread; widespread rain, however, may contain convective cells having a high rain rate, so on an average the rain rate along the total path will be higher than that at a point. For high rain rates the rain tends to be localized, so the average rain rate for the total path would ordinarily be lower than that at a point. As expected, the correction factor is heavily dependent on the path length.

In Section II.B.3.a the aR^b relationship for attenuation as a function of rain rate was introduced. By using the path average rain rate concept of the previous paragraph it is possible to derive a correction term for the aR^b expression. From Crane (1980b), we have

$$A(R_p, D) = aR_p^\beta \left(\frac{e^{u\beta d} - 1}{u\beta} - \frac{b^\beta e^{c\beta d}}{c\beta} + \frac{b^\beta e^{c\beta D}}{c\beta} \right), \quad d \le D \le 22.5 \text{ km}, \tag{24}$$

$$= aR_p^\beta \left(\frac{e^{u\beta D} - 1}{u\beta} \right), \qquad 0 < D \le d, \tag{25}$$

where R_p is in millimeters per hour, D in kilometers, the specific attenuation $A(R_p, D)$ in decibels per kilometer, and

$$u = \ln(be^{cd})/d, \qquad b = 2.3R_p^{-0.17},$$

$$c = 0.026 - 0.03 \ln R_p, \qquad d = 3.8 - 0.6 \ln R_p.$$

For $D > 22.5$ km, the probability of occurrence P is replaced by a modified probability of occurrence

$$P' = (22.5/D)P. \tag{26}$$

For example, suppose that for a particular climatic region the rain rate exceeds 28 mm/h 0.01% of the time and 41 mm/h 0.005% of the time ($R_{0.01} = 28$ mm/h, $R_{0.005} = 41$ mm/h. The attenuation along a 22.5-km path that would be exceeded 0.01% of the time can be calculated directly from Eq. (24) or (25). To determine the attenuation that would be exceeded 0.01% of the time over a 45-km path, a new percentage of time $P' = (22.5/45)P = 0.005\%$ would be used, with a corresponding rain rate of $R_{0.005} = 41$ mm/h. Now the attenuation that would be exceeded 0.01% of the time for a 45-km path would be based on a rain rate of $R_{0.005} = 41$ mm/h for a 22.5-km path.

To improve the reliability of a terrestrial link, path diversity can be utilized. As mentioned previously, the heavy rain that has a severe impact on terrestrial link performance tends to be localized. By using redundant

terminals, the probability of having a path free from heavy rain is increased. Ideally, the optimum separation of transmitter or receiver terminals (or both) is that for which the rain rates (and corresponding attenuations) for the pair of terminals are uncorrelated. This separation is a function of the climate and rain rate. Blomquist and Norbury (1979) have studied diversity improvement for a number of paths with lengths of about 3–to 13 km and terminal separations of 4–12 km. Based on very limited data, they found that the diversity improvement increased as the terminal separation was increased from 4 to about 8 km; there was, however, no additional improvement as the separation was increased further. Because only limited statistical data on diversity advantage are presently available, it is not possible to determine optimal terminal spacings for most locations. However, there is sufficient evidence to indicate that a diversity mode of operation can significantly improve the performance of line-of-sight links.

2. *Terrain Scatter and Diffraction*

If the terminals of a line-of-sight path are close to the surface, then propagation losses due to both multipath and diffraction are possible. These mechanisms were described in Sections II.A.3.b and II.A.4, respectively, and it was seen that the multipath or diffracted signal can interfere with the direct signal; the net effect is a resultant signal that may vary in amplitude from zero intensity to twice the intensity of the direct signal. It should be emphasized that the interference is strongest when the multipath or diffracted signal is coherent. For multipath this occurs when the terrain is smooth with respect to wavelength; for diffraction it occurs from a prominent obstacle or a set of obstacles that happen to add constructively (or destructively).

Regarding terrain muiltipath, even though most terrains have surface irregularities much larger than 1 mm, we see from Eqs. (9) and (10) that as the grazing angle becomes small the surface becomes electromagnetically smooth (the reflection coefficient approaches unity) and large specular signals are possible. These signals interfere with the direct signal and can significantly degrade the performance of a line-of-sight system. Hayes *et al.* (1979) have made multipath measurements over grass and snow at wavelengths of 8.6, 3.1, and 2.1 mm and obtained height–gain curves with nulls in excess of 20 dB, the nulls being deeper for snow cover than for grass and also deeper at longer wavelengths. Measurements were made for both vertical and horizontal polarizations; because grazing angles were well below the Brewster angle, the height–gain curves were similar for both polarizations.

Interference effects produced by a diffracted signal should not be as large as those produced by multipath, because the obstacles that would diffract

the wave are not likely to produce a coherent signal. As mentioned previously, if the surface irregularities of a prominent obstacle are rough with respect to wavelength, there are many uncorrelated, diffracted rays and the resultant signal consists of a diffuse signal superimposed upon a weak specular signal; if the surface is very rough the specular component will disappear. Also, it is seen from Eq. (14) that the direct path must be within meters of the top of the obstacle for a diffracted signal to appear. However, diffracted signals have been measured at frequencies as high as 28.8 GHz (Haakinson *et al.*, 1980), so this phenomenon is certainly possible at millimeter wavelengths under the "right" conditions.

3. *Depolarization*

As mentioned in Sections II.A.5 and II.B.2, depolarized signals may arise from either multipath or precipitation. A multipath ray obliquely incident on a paraboloidal receiving antenna can produce a cross-polarized component. Oblate rain drops canted with respect to the plane of the polarization vector of the incident wave also produce a cross-polarized component. The net effect is that the resultant signal is depolarized and the system performance compromised. Vander Vorst (1979) has summarized the effects of depolarization on line-of-sight links. Measurements on a 53-km terrestrial path have shown that depolarization produced by multipath has a more severe effect on link performance than that produced by rain (Rooryck and Battesti, 1975). The influence of rain caused only a very small degradation of the performance of a dual-polarized system with respect to a single-polarization system, whereas the same was not true for multipath.

4. *Refraction and Atmospheric Multipath*

Under normal atmospheric conditions an electromagnetic wave is bent towards the earth's surface. The amount of bending is proportional to the length of the path, so for long paths refractive bending corrections may be required, as discussed in Section II.A.1.c. Under abnormal atmospheric conditions—for example, those producing a sharp negative gradient in the refractivity as a function of height—the wave may become trapped (ducting) or a multipath signal may be produced by the "layer" arising from the refractivity structure. Although refraction and multipath effects are possible in principle, they are not considered important as far as millimeter-wave line-of-sight links are concerned, because, as mentioned previously, attenuation effects will normally prohibit the use of very long paths.

B. Earth–Space Paths

For earth–space paths, propagation effects become more severe with decreasing wavelength. For elevation angles above about 6°, attenuation and

emission from atmospheric gases and precipitation are of principal concern. In addition, backscatter and depolarization resulting from precipitation may also cause problems. For low elevation angles all of the problems associated with long terrestrial paths are present. The determination of propagation effects for slant paths is generally more difficult than for terrestrial paths. The modeling of a slant path under conditions of cloud and precipitation is particularly complicated, because the structure of the particulates is varying in both time and space. Experimentally, it is very expensive to place a millimeter-wave beacon on a satellite or aircraft, so other means of obtaining attenuation information are often used.

1. *Attenuation and Emission*

Atmospheric attenuation and emission are the most serious propagation problems for earth–space systems. Because the attenuation decreases the signal level and the emission (or effective noise temperature) sets a minimum noise level for the receiver, the only way to maintain the system signal-to-noise ratio is through increased transmitter power or a diversity mode of operation. High powers are not readily available at millimeter wavelengths and diversity systems are costly, so these options have their difficulties.

For clear sky conditions, the attenuation is a function of oxygen and water vapor density along the path. The vertical distributions of these gases are assumed to decrease exponentially with height and have scale heights of approximately 4 and 2 km, respectively. The zenith attenuation as a function of wavelength can be estimated from (CCIR, 1982b)

$$A_{90^\circ} = \alpha + \beta\rho_0 - \xi T_0. \tag{27}$$

The coefficients α, β, and ξ are plotted in Fig. 15. The attenuation at elevation angles above about 6° can be calculated by multiplying the zenith attenuation by the cosecant of the elevation angle. For angles below 6° the attenuation is assumed to be proportional to the path length through the attenuating medium. This distance is given by (Altshuler *et al.*, 1978)

$$d(\theta) = [(a_e + h)^2 - a_e^2 \cos^2\theta]^{1/2} - a_e \sin\theta, \tag{28}$$

where θ is the elevation angle, a_e ⅘ the earth's radius (8500 km), and h the scale height of combined oxygen and water vapor gases ($\sim$ 3.2 km). Therefore,

$$A(\theta) = A(90^\circ)d(\theta). \tag{29}$$

The zenith attenuation is plotted as a function of wavelength in Fig. 16 for a completely dry atmosphere and more typical atmospheres having surface absolute humidities of 3 and 10 g/m³ (Smith, 1982). For a dry atmosphere

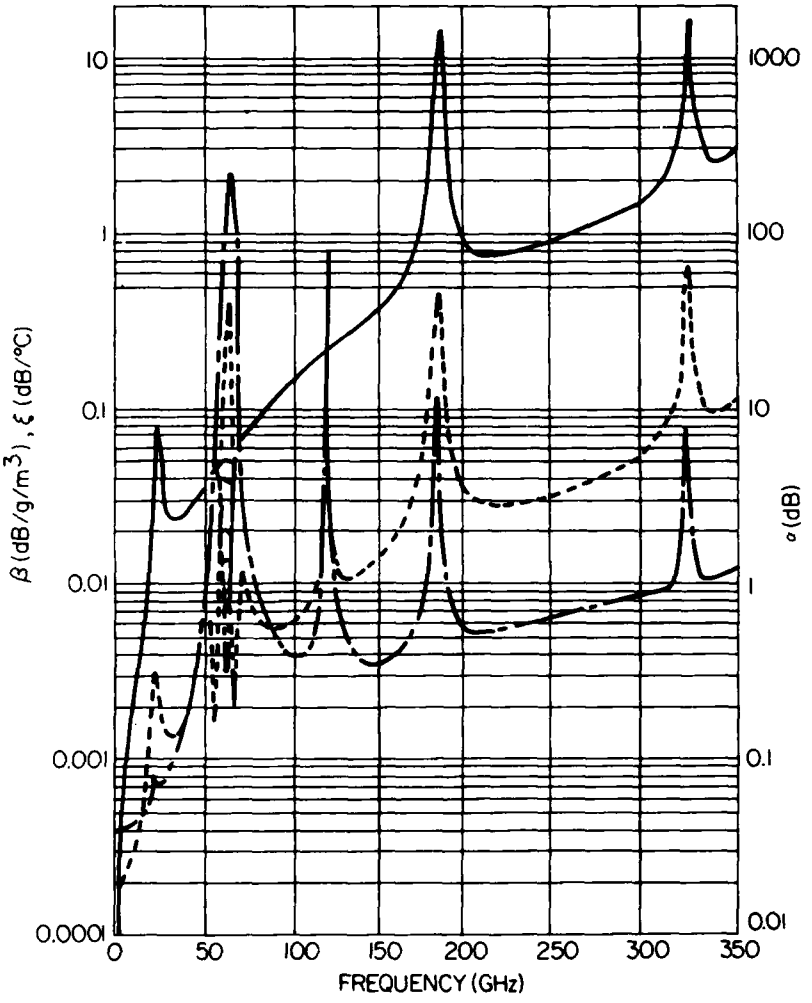

FIG. 15 Coefficients for computing zenith attenuation. Zenith attenuation $\tau_{90^\circ} = \alpha + \beta\rho_0 - \xi T_0$ (dB), with ρ_0 in grams per cubic meter and T_0 in degrees Celsius: — · —, α coefficient; ——, β coefficient; – – –, ξ coefficient. (From CCIR, 1982b).

the total zenith attenuation in the window regions is only a fraction of a decibel per kilometer. However, this attenuation increases very sharply as the atmosphere becomes moist, particularly below a wavelength of a few millimeters, at which losses on the order of tens of decibels are possible. A plot of the apparent sky temperature (emission) is shown in Fig. 17 as a function of frequency for a set of elevation angles from the horizon to zenith and for an atmosphere having a water vapor density of 7.5 g/m³ (Smith, 1982). The sky temperature is relatively low for higher elevation angles and

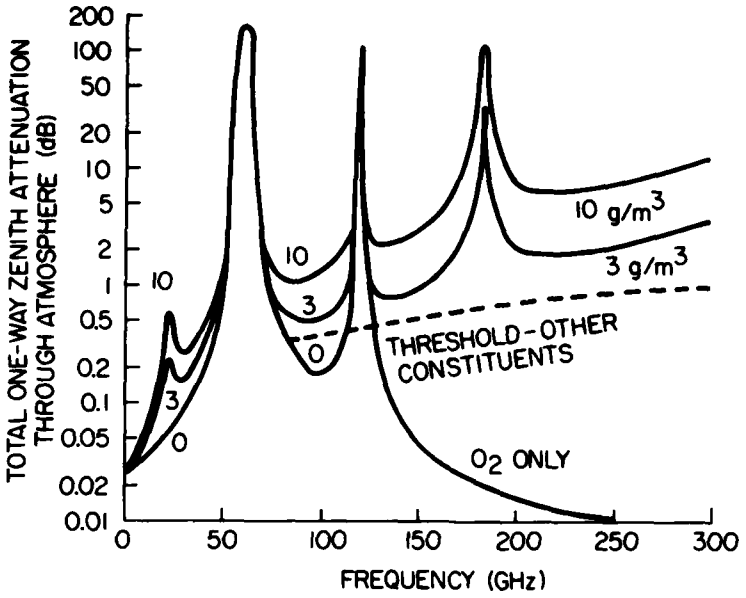

FIG. 16 Total zenith attenuation through atmosphere as a function of frequency. (From Smith, 1982. © American Geophysical Union.)

longer wavelengths and gradually increases for lower elevation angles and shorter wavelengths, approaching a terrain temperature of approximately 290 K.

For conditions of fog or cloud, the modeling of the atmosphere becomes increasingly difficult, particularly for slant paths close to the horizon. Fog and cloud models have been developed, however (Falcone *et al.*, 1979), and in principle the attenuations can be calculated using the information provided in Fig. 13. It must be emphasized that these attenuations are only approximate, because neither the true liquid water density of the cloud nor the extent of the cloud is accurately known. Because the cloud particulates are in the Rayleigh region and scattering losses are negligible, the corresponding brightness temperature (emission) can be calculated from Eq. (6).

Several investigators have measured cloud attenuations at millimeter wavelengths. Altshuler *et al.* (1978) have presented cloud attenuation statistics at frequencies of 15 and 35 GHz based on 440 sets of measured data. They characterized sky conditions as clear, mixed clouds, or heavy clouds. Average attenuations as a function of elevation angle are shown in Fig. 18. They also demonstrated a reasonable correlation between the slant path attenuation and surface absolute humidity. Typical slant path attenuations extrapolated to zenith were 0.1 and 0.36 dB at 15 and 35 GHz, respectively. Lo *et al.* (1975) measured attenuations at wavelengths of 8.6 and 3.2 mm

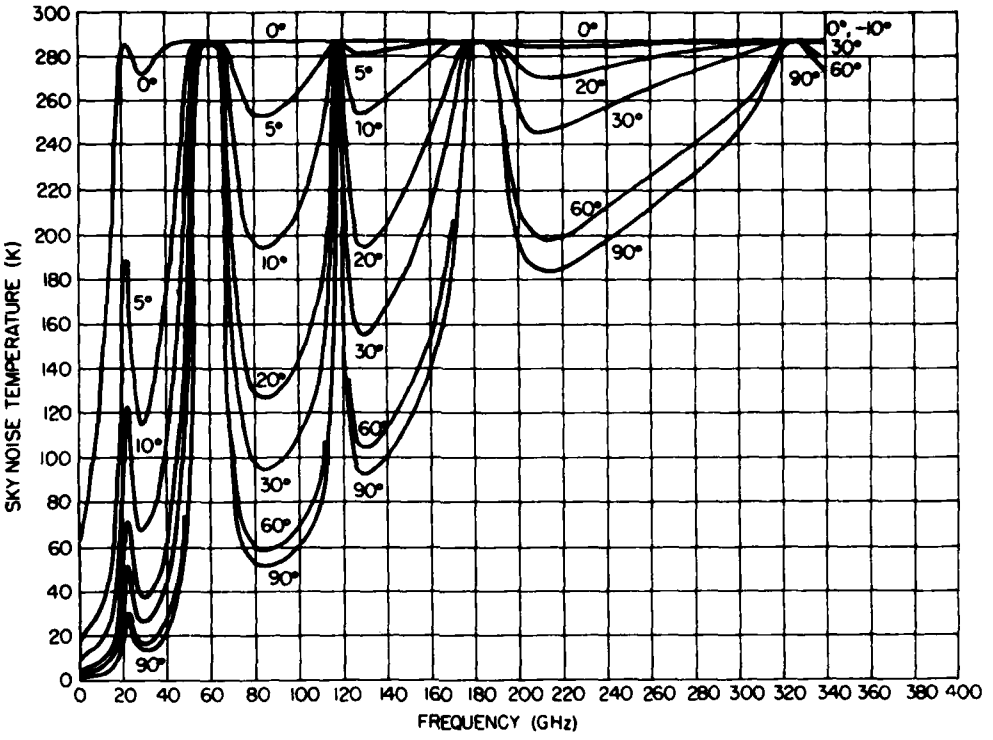

FIG. 17 Sky noise temperature as a function of frequency for a water vapor density of 7.5 g/m³. (From CCIR, 1982).

over a 6-month period, and obtained typical attenuations of 0.42 and 2.13 dB, respectively. Slobin (1982) has estimated average-year statistics of cloud attenuation and emission down to a wavelength of 6 mm for various climatically distinct regions throughout the United States.

As was the case for terrestrial paths, rain, sleet, and wet snow present the most serious propagation limitations on earth–space millimeter-wave systems. A number of investigators have derived models for predicting rain attenuation, and their results have been summarized by Ippolito (1981). All of the techniques assume that the slant path attenuation can be estimated by modifying the attenuation for a terrestrial path by an effective path-length parameter that is usually a function of the elevation angle and the type of rain. For example, the Crane (1980b) model for estimating rain attenuation for terrestrial paths, presented in Section III.A.1, can be modified for slant path attenuations. It is assumed that the rain rate has a constant value between the station height h_0 and the height h of the 0°C isotherm. Precipitation above the 0°C isotherm consists of ice particles, so the attenuation is considered negligible. Although the height of the 0°C isotherm is variable, radar measurements have shown it to have a strong dependence on site

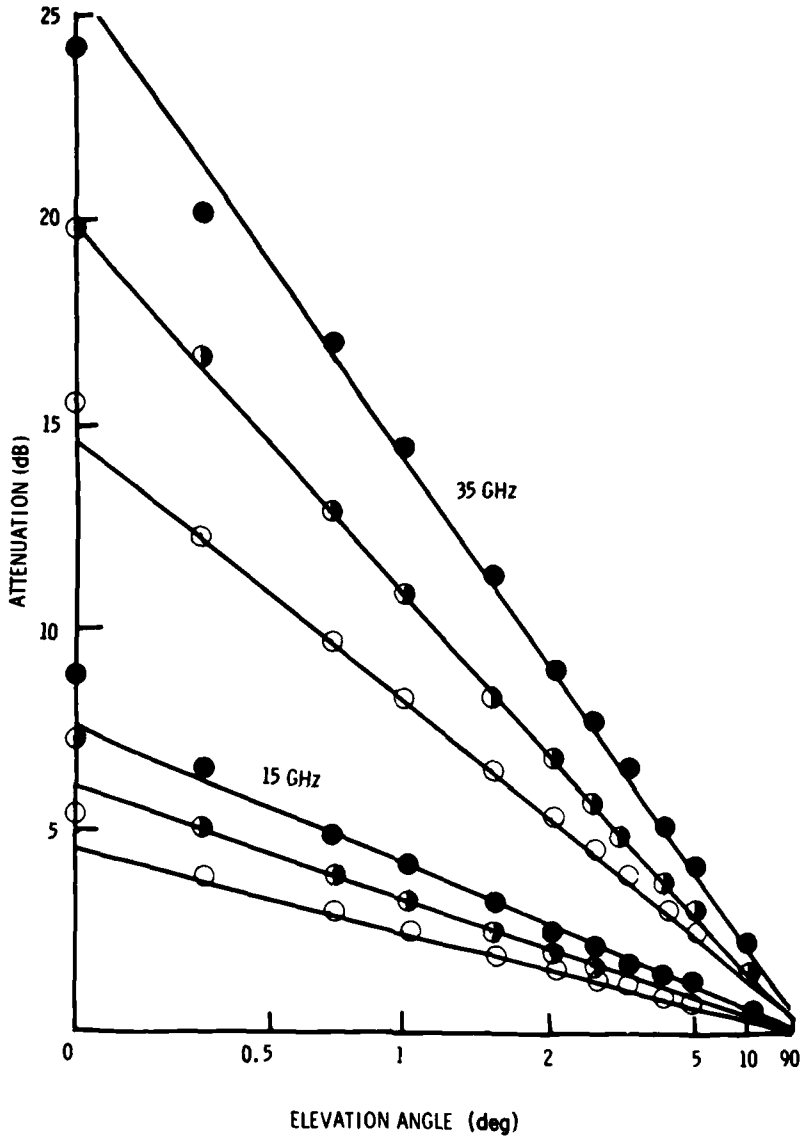

FIG. 18 Typical cloud attenuations as a function of elevation angle: ○, clear; ◑, mixed; ●, cloudy. (From Altshuler *et al.*, 1978. © Published by the American Geophysical Union.)

latitude and rain rate, which in turn are linearly related to the logarithm of the probability of occurrence P; Crane (1980b) has derived a set of curves for estimating the height h, and these are shown in Fig. 19. With h and h_0 known, the effective path length D through the rain can be calculated:

$$D = (h - h_0)/\tan\theta, \qquad \theta \geq 10^\circ, \tag{30}$$

$$= a_e\psi, \qquad \theta < 10^\circ, \tag{31}$$

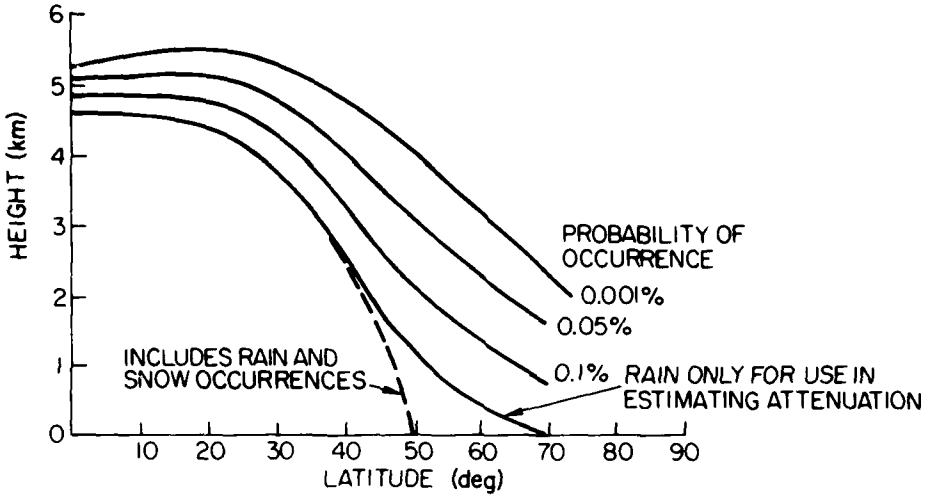

FIG. 19 0°C isotherm height for use in estimating the depth of the attenuating region on a slant path. (From Crane, 1980b. © 1980 IEEE.)

where

$$\psi = \sin^{-1}\left(\frac{\cos\theta}{h + a_e}\{[(h_0 + a_e)^2 \sin^2\theta + 2a_e(h - h_0) + h^2 - h_0^2]^{1/2} - (h_0 + a_e)\sin\theta\}\right), \tag{32}$$

a_e is the effective earth radius (8500 km), and θ is the elevation angle.

The surface-projected attenuation $A(R_p, D)$ is calculated from Eq. (24) or Eq. (25). Then, the value for the slant path A_s is estimated assuming a constant attenuation below h by

$$A_s = LA(D)/D, \tag{33}$$

where

$$L = D/\cos\theta, \quad \theta \geq 10° \tag{34}$$

$$= [(a_e + h_0)^2 + (a_e + h)^2 - 2(a_e + h_0)(a_e + h)\cos\psi]^{1/2}, \quad \theta < 10°. \tag{35}$$

Several methods can be used to measure slant path attenuations. The most straightforward, but also most costly, is to place a millimeter-wave beacon in space. Measurements using satellite beacons have been made at wavelengths from approximately 30 to 10 mm and have been summarized by Ippolito (1981). A number of investigators have made attenuation measurements using the sun as a source (Altshuler and Telford, 1980; Davies, 1973; Wilson, 1969; Wulfsberg, 1967). When a radiometer is pointed at the sun, the noise power received consists of radiation from the sun and the atmosphere. The antenna temperature can be expressed as

$$T_a = T'_a e^{-\tau} + \int_0^\infty T(s)\gamma(s) \exp\left(-\int_0^\infty \gamma(s')\, ds'\right) ds, \tag{36}$$

where T'_a is the effective antenna temperature of the sun with no intervening atmosphere (in degrees Kelvin), $T(s)$ the atmospheric temperature, τ the total attenuation (in nepers), $\gamma(s)$ the absorption coefficient, and s the distance from the antenna (ray path). In simpler terms

$$T_a = T'_a e^{-\gamma} + (1 - e^{-\gamma})T_m, \tag{37}$$

where T_m is the atmospheric mean absorption temperature within the antenna beam. The attenuation γ appears in both terms on the right-hand side of Eq. (37). Because the second term is the emission, it can easily be canceled out by pointing the antenna beam toward and away from the sun. With the second term balanced off, Eq. (37) can be solved for γ, converted from nepers to decibels, and expressed as

$$A = 10 \log(T'_a/T_a). \tag{38}$$

T'_a is determined from a set of antenna temperature measurements made under clear sky conditions as a function of elevation angle; for these conditions the antenna temperature is proportional to the cosecant of the elevation angle, and it can be shown that T'_a is equal to the slope of the line log T_a versus csc θ (Wulfsberg, 1967).

Because the attenuation also appears in the emission term in Eq. (37), it is possible to determine the attenuation from an emission measurement. In this method the antenna must be pointed away from the sun or the moon (millimeter-wave radiation from all other natural sources is negligible), so the first term on the right-hand side of Eq. (37) can be considered zero and Eq. (37) reduces to Eq. (5). As before, the equation is then solved for the attenuation γ and expressed in decibels as

$$A = 10 \log T_m/(T_m - T_a).$$

Another technique for estimating rain attenuation at millimeter wavelengths is from a measurement of the reflectivity factor of the rain. Attenuation is derived from established relationships between these parameters (Goldhirsh, 1979). When a single-wavelength radar is used, calibration errors and the uncertainty in the reflectivity–attenuation relationship, particularly for mixed phase precipitation, limit the accuracy of this technique. Uncertainties in the reflectivity–attenuation relationship can, however, be reduced by using a dual-wavelength radar and measuring the differential attenuation.

In summation, there are four methods for measuring slant path attenuations. The most direct method is to place a source in space. This allows measurements to be made over a very wide dynamic range. An additional

advantage is that the polarization and bandwidth limitations imposed by the atmosphere can also be measured. One disadvantage is cost; and, depending on the satellite orbit, measurements may be possible at only one elevation angle, which may or may not be a drawback. Total attenuation can be measured very accurately and economically using the sun as a source over dynamic ranges approaching 25–30 dB. A disadvantage is that measurements can be made only in the direction of the sun and during the day.

Attenuation can easily be determined from an emission measurement on a continual basis and at any elevation angle. It must be emphasized that there are two major problems that limit the accuracy of this technique. The true value of T_m is not always known; if $T_m - T_s$ is large this uncertainty is not serious, but if $T_m - T_s$ is small a large error may arise. Also, the emission is related only to the absorption, whereas the attenuation includes losses due to scattering in addition to those due to absorption. Therefore, in cases for which the Rayleigh approximation is not valid and scattering losses are appreciable, errors will arise. Techniques for correcting for the additional losses due to scattering have been investigated by Zavody (1974) and Ishimaru and Cheung (1980). For these reasons this method is not generally recommended for attenuations much above 10 dB.

Attenuations determined from radar reflectivity measurements have the limitations in accuracy discussed previously, and in general this technique is not suitable for losses arising from very small particulates such as fog, cloud, or drizzle. This method does, however, have the advantage of measuring attenuation as a function of distance from the transmitter. McCormick (1972) has compared attenuations derived from radar reflectivity with those obtained directly utilizing a beaeon placed on an aircraft. Strickland (1974) has measured slant path attenuations using radar, radiometers, and a satellite beacon simultaneously.

C. Transhorizon Paths

Very little is known about transhorizon propagation at millimeter wavelengths. Although a large number of troposcatter, tropospheric ducting, and diffraction experiments have been conducted over the years, they have been limited to wavelengths on the order of centimeters and longer. Based on the results that have been obtained, coupled with theoretical findings, empirical relationships for estimating path losses have been derived (CCIR, 1978). Under normal atmospheric conditions and for paths just slightly beyond the horizon, the diffracted field is the largest, particularly if the diffracting terrain approximates a knife edge. As the distance beyond the horizon is increased, the received signal consists of both diffracted and troposcatter components. For still longer distances, the diffracted field disappears and the received signal is entirely troposcatter. Finally, for very long paths, tropo-

spheric ducting is possible; however, it must be emphasized that this is an anomalous mode of propagation that occurs only for the special refractivity structure described in Section II.A.1.a.

In principle, troposcatter, tropospheric ducting, and diffraction modes of propagation are all possible at millimeter wavelengths. Traditionally, transhorizon propagation has been used for paths hundreds of kilometers in extent. However, this is not practical at millimeter wavelengths, because these modes of propagation occur only for very low elevation angles and atmospheric attenuation is large, particularly for shorter millimeter wavelengths. Although the advent of satellite communications has reduced the need for transhorizon systems, there are still potential applications for paths only slightly beyond the horizon.

1. *Troposcatter*

The principal advantages of using millimeter wavelengths for troposcatter are smaller antennas and larger available bandwidth. Parl and Malaga (1982) have calculated the path loss for a troposcatter system using turbulence scatter theory and obtained the results plotted in Fig. 20, which shows the received signal level as a function of frequency for several water vapor pressures. The calculations are based on transmitting and receiving antennas with 15-ft. apertures placed 100 km apart. It is interesting to note that the received signal level increases slowly with frequency up to about 12 GHz, at which point the aperture-to-medium coupling loss and atmospheric attenuation begin to outweigh the additional antenna gain due to a fixed-size aperture and shorter wavelength. In addition, the signal level increases significantly with higher water vapor pressures, because the refractive structure constant C_n^2 becomes higher. Although signal levels above 12 GHz drop off with increasing frequency, they are still high enough to be easily detected. The presence of precipitation along the path has two effects: it enhances the scattering but also attenuates the signal. The additional scattering, however, is not always an advantage, because it can produce intersystem interference (Crane, 1981).

Because the troposcatter mechanism is one of scattering from a turbulent medium, the field across the receiving aperture is not always a plane wave, and thus the gains of the transmitting and receiving antennas do not necessarily correspond to the plane-wave antenna gains. This loss in gain is the aperture-to-medium coupling loss, defined as the ratio of the power that would be received if the plane-wave gain of each antenna were realized to the power actually received (Waterman, 1958). This aperture-to-medium coupling loss increases as the beamwidths of the antennas decrease; thus the net gain of a troposcatter system does not increase proportionally with increasing antenna aperture. Likewise, the high gains that can be achieved with

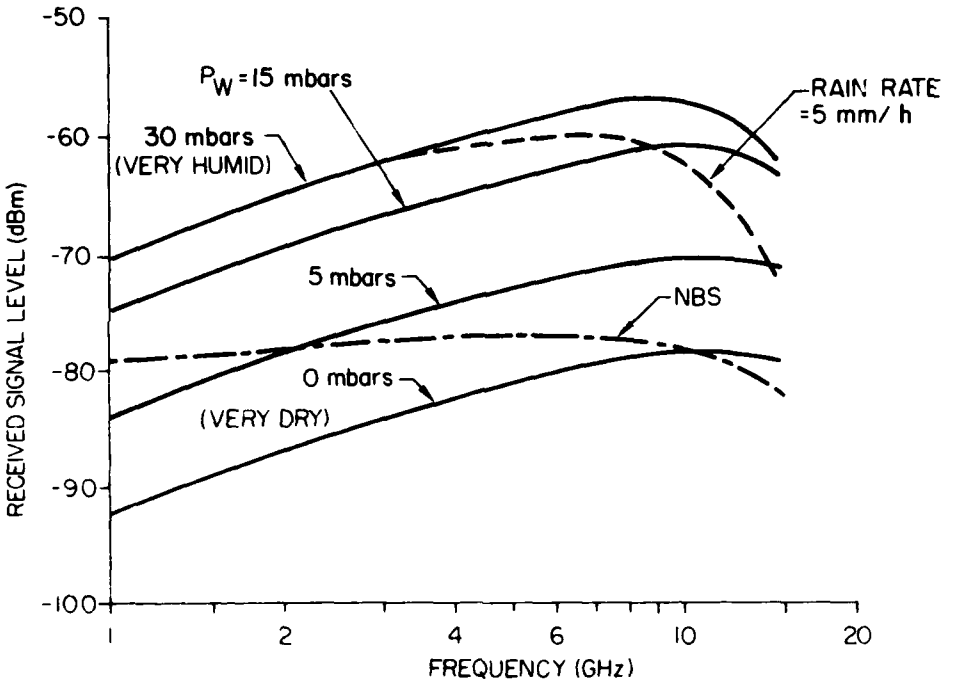

FIG. 20 Received signal level of troposcatter link compared to the National Bureau of Standards signal level. Based on 15-ft. antennas in a 100-km path. P_T = 100 W. (From Parl and Malaga, 1982.)

antennas of moderate size at millimeter wavelengths do not automatically translate into higher system gains. Unfortunately, the aperture-to-medium coupling loss is a complex function of the refractive index structure constant within the common volume, which is defined by the intersection of the antenna beams, and this is not easily determined; thus it is still not possible to predict this loss with any degree of confidence (Gough, 1968).

Another problem that arises from the nature of the scattering medium is fading of the received signal. Slow fades (of the order of hours) are usually attributed to major changes in the refractive index structure produced by changes in the weather. Fast fades (on the order of seconds) are attributed to the fact that the received field consists of many incoherent contributions from scatterers within the common volume.

Aperture-to-medium coupling loss and fading can be compensated for using diversity techniques. In this mode of operation the system is designed so that at least two essentially independent signals are received and then combined in an optimal way. The most common types of diversity are space (separate apertures), angle (separate feeds with common aperture), and frequency (separate frequencies). Empirical relationships for these separa-

tions have been derived and are summarized in CCIR (1978). At millimeter wavelengths, phased arrays are being considered for troposcatter systems. Because the amplitude and phase across this type of aperture can be controlled, more sophisticated diversity techniques are possible.

2. *Tropospheric Ducting*

Although it is possible to transmit over very long distances in a ducted mode, the fact that ducting occurs sporadically, depending upon location, time of day, season, etc., makes it of little use for transhorizon propagation applications. Ducting is usually of concern because it produces radio or radar holes (regions of weak signal level in the desired direction) and thus degrades system performance. Unfortunately, there is in general no way of preventing ducting, although changing the heights of the transmitter or receiver may sometimes help. Methods for detecting the presence of a duct or, better yet, for predicting the onset of a duct are being pursued. Because ducting is most likely to occur only for very low elevation angles, it should

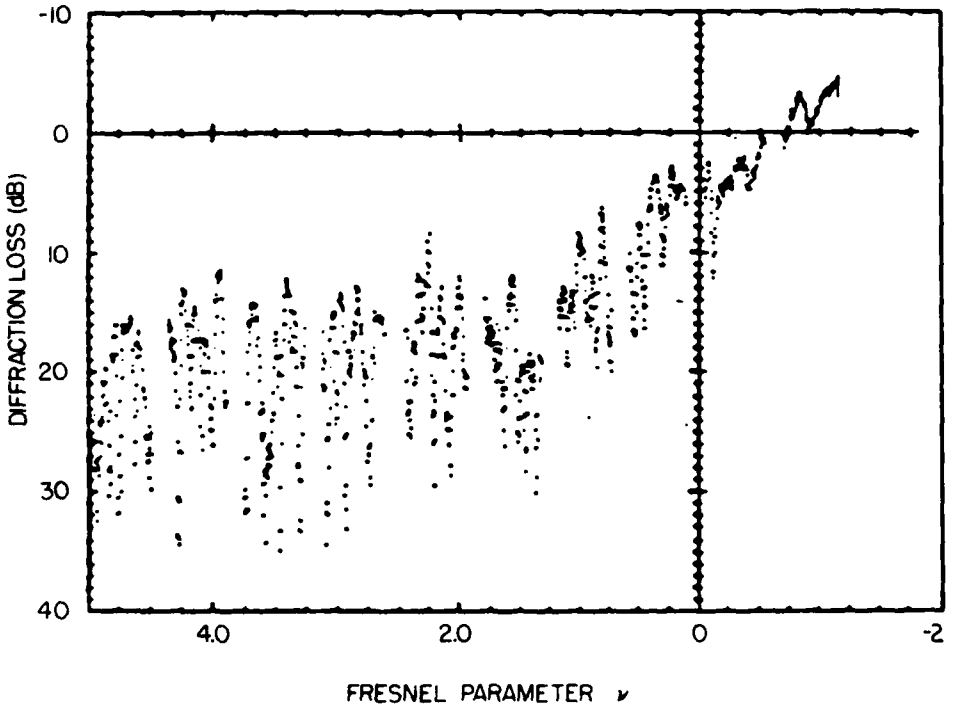

FIG. 21 Diffraction loss measured on a cluttered path with multiple diffraction. (From Haakinson *et al.*, 1980. © Reproduced by permission of the U.S. Dept. of Commerce, National Technical Information Service, Springfield, Virginia 22161.)

not normally be a problem at millimeter wavelengths, because atmospheric attenuation ordinarily prevents the use of these very low angles.

3. *Diffraction*

The diffraction mechanism described in Section II.A.4 may be a viable mode of propagation for paths slightly beyond the horizon, particularly if the diffracting terrain approximates a knife edge. However, diffraction effects are not limited to simple obstacles; for example, irregular terrain can produce a diffraction loss at frequencies as high as 28.8 GHz (Haakinson *et al.*, 1980). At millimeter wavelengths a statistical approach is used, and the diffraction loss is viewed as the superposition of many ray paths diffracted from these obstacles. The diffraction loss produced by trees on a smooth hill at 28.8 GHz is plotted in Fig. 21 (Haakinson *et al.*, 1980); this loss has a mean behavior of a single obstacle with random variations superimposed. Thus diffraction effects can occur at millimeter wavelengths, but are found to be of less importance than those at longer wavelengths. Also, theoretical solutions for natural terrains are not generally possible, because at these wavelengths the obstacles cannot be considered smooth.

IV. Remote Sensing of the Atmosphere

Because of the strong interaction between millimeter waves and atmospheric gases and particulates, the propagated wave can serve as a diagnostic tool for sensing the meteorological properties of the atmosphere. In particular, it is possible to infer information on temperature, water vapor, turbulence structure, wind velocity, cloud composition and dynamics, and rain distribution and intensity. In addition, even a nonmeteorological application such as insect detection may prove to be a valuable use of millimeter-wave sensing.

Three types of systems are used for remote sensing: line-of-sight, radiometric, and radar. Line-of-sight systems consist of a transmitter and a receiver and probe the intervening atmosphere. Radiometric systems measure the atmospheric emission (or brightness temperature) of the atmosphere. Radar systems measure the reflective properties of atmospheric particulates or the refractive index structure. Radiometric and radar sensors may be either ground based (directed upward) or space-borne (directed downward). In addition, it is often advantageous to use a hybrid system that has both radiometric and radar channels.

A. Line-of-Sight Transmission

In this section we shall review methods for inferring the composition and structure of the atmosphere between a transmitter and a receiver. For a clear

atmosphere, two parameters can be inferred from millimeter-wave measurements: the refractive index structure constant C_n^2 and the wind velocity. A method for inferring average raindrop size is also described.

1. *Refractive Index Structure Constant*

As mentioned in Section II.A.1.e, the atmosphere has a fine scale refractive index structure that varies both temporally and spatially, and the strength of this structure is characterized by the parameter C_n^2. These variations produce amplitude and phase fluctuations across the wave front of the transmitted signal. In practice, the receiving antenna would be an array transverse to the propagated wave. It has been shown theoretically that the covariances of the fluctuations are related to the structure constant C_n^2; thus the wave front is sampled at each array element, the covariances are calculated, and C_n^2 is determined by inverting the integral that relates these quantities (Leuenberger *et al.*, 1979; Shen, 1970). In principle, it should be possible to obtain the distribution of C_n^2 along the entire path; however, this has not yet been demonstrated, primarily because of the low degree of accuracy with which the integral can be inverted. Average values of C_n^2 for the whole path, however, have been obtained.

2. *Wind Velocity*

The procedure for determination of the wind velocity across the path is very similar to that used to obtain C_n^2. For this case one is interested in the shape of the time-lagged coveriance function, determined by measuring the signal fluctuations at each array element and computing the covariances for a set of time delays. Once again the wind velocity is calculated by inverting the integral that relates the time-lagged covariance to C_n^2 (Leuenberger *et al.*, 1979; Shen, 1970). As for the case of C_n^2, attempts to calculate the average wind velocity have been more successful than those to calculate the distribution of wind velocity along the path.

3. *Raindrop Size Distribution*

In Eq. (20) the rain attenuation is a function of the integral of the drop size distribution $N(D)$. In principle, if the path attenuation is measured at a number of wavelengths it is possible to invert this integral and determine the path-averaged raindrop size distribution $\overline{N(D)}$. Furuhama and Ihara (1981) measured copolar attenuations at 11.5, 34.5, and 81.8 GHz and phase variations between the frequencies 11.5 and 34.5 GHz and then inferred $\overline{N(D)}$ from these data. They compared the results obtained using several different inversion techniques with actual drop size distributions measured with a distrometer and found that the best results were obtained if the drop diameters were considered to be distributed exponentially. The inferred

average drop size distribution was in good agreement with distrometer measurements over the range of drop diameters 1.5–3.5 mm, but the number of smaller and larger drop sizes was grossly overestimated. The authors conclude from these initial results that this technique appears feasible for remotely sensing the path-averaged raindrop size distribution.

B. Radiometric Sensing

In Eq. (5) the atmospheric emission (or sky brightness temperature T_a) is a function of the kinetic temperature of the atmosphere $T(s)$ and the absorption coefficient of the absorbing gases $\gamma(s)$; $\gamma(s)$ is in turn a function of temperature, pressure, water vapor pressure, wavelength, and elevation (or nadir) angle. If the distribution of an absorbing gas is known, remains reasonably constant, and is sufficiently abundant, as is the case for oxygen, then Eq. (5) can be inverted and in principle a temperature profile $T(s)$ can be inferred from a set of brightness temperature measurements as a function of wavelength (or elevation angle).

Remote sensing of the atmosphere may be conducted with a ground-based system directed upward (Hogg, 1980) or a satellite or aircraft system directed downward (Staelin, 1981). For the downward-directed system an additional surface contribution must be added to Eq. (5). This is usually negligible for temperature profiles but it is very important in water vapor and liquid water measurements. The procedure for retrieving meteorological data from atmospheric emission measurements is similar for both ground-based and satellite systems. A concept that enables the best understanding of the inversion technique is that of the weighting function. Equation (5) can be written in the form

$$T_a = \int T(h)W(h, v)\, dh, \tag{39}$$

where $W(h, v) = \gamma(h) \exp[-\int \gamma(h')\, dh']$. The kernel of this integral, $W(h, v)$, is called the weighting function because it represents the contribution from each height interval to the total emission. The height distribution of the weighting function is a function of frequency; thus by varying frequency one can sample the emission from different heights. Typical weighting functions for temperature sensors directed downward and upward are shown in Figs. 22 and 23, respectively (Miner, 1972; Waters *et al.*, 1975). The closer the frequency is to the peak of the absorption line, the closer the layer from which the emission is emanating, is to the antenna, because emissions from layers distant from the antenna are absorbed before reaching the antenna. Whereas the downward-directed weighting functions peak at different heights, those directed upward all peak at the surface, because the density of oxygen decreases with height and, therefore, in the upward direction emission is always greatest at the antenna.

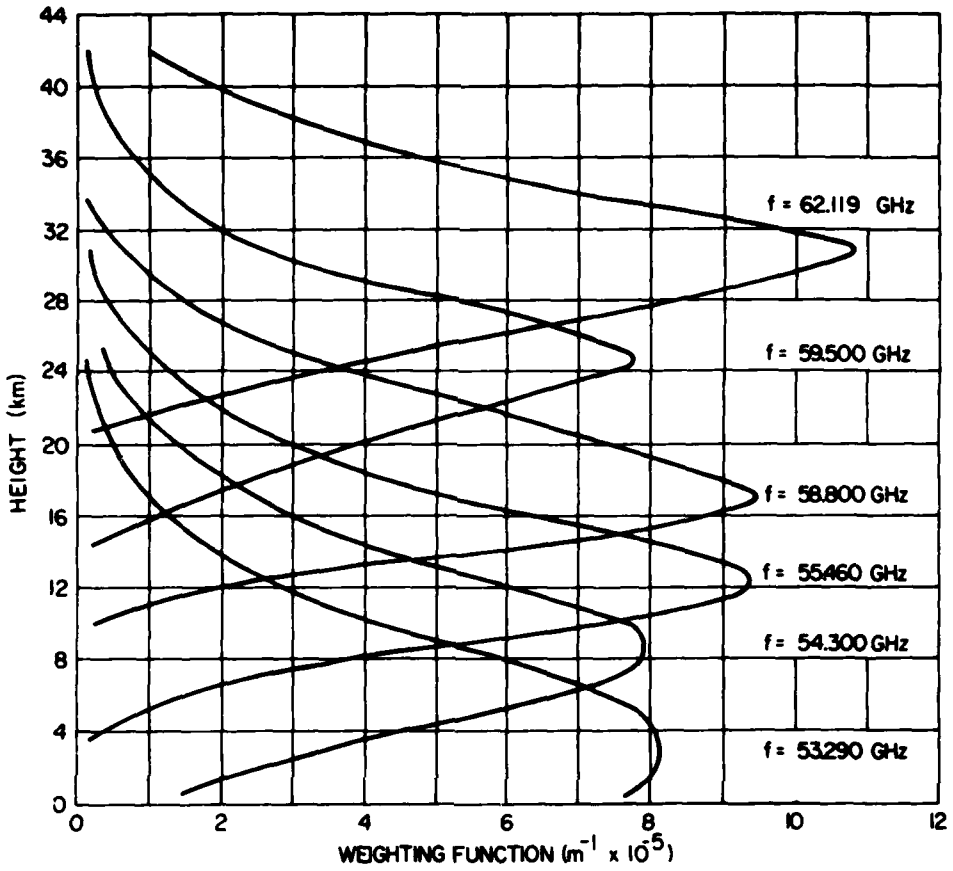

FIG. 22 Normalized temperature weighting functions for downward-directed temperature sensors for four frequencies (——) and the corresponding temperature profile (---). (From CCIR, 1982.)

Temperatures at discrete heights can be estimated from a set of brightness temperature measurements, because these temperatures are correlated with the temperature over the weighting function layer. Because the correlation is imperfect, the vertical resolution of the temperature profile is limited. There are, in addition, several uncertainties that further limit the accuracy of the inversion technique. First, this type of integral, often referred to as a Fredholm integral of the first kind, is unstable; that is, very small errors in the measurement of the brightness temperature, or in the accuracy with which the absorption coefficient of oxygen is known, can give rise to very large errors in the inferred temperature profile. Also, although wavelengths can be selected such that most of the absorption is due only to oxygen, contributions from water vapor and clouds further limit the accuracy of this technique. Methods for overcoming these limitations will be discussed later.

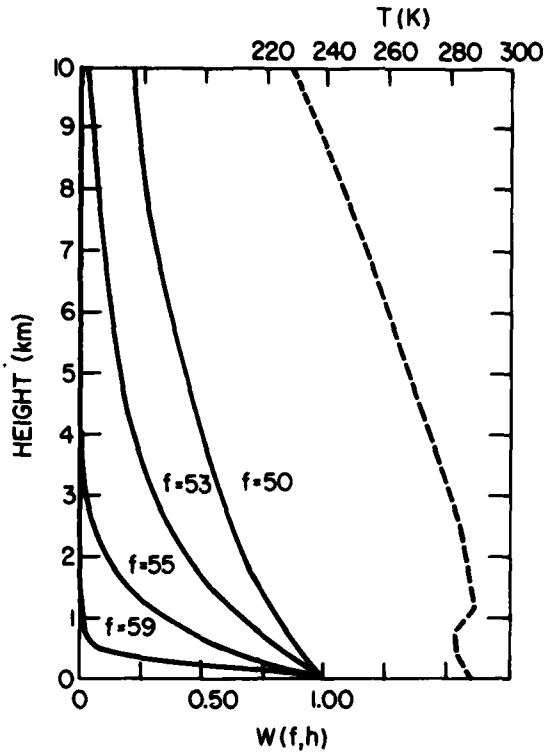

FIG. 23 Weighting functions for upward-directed temperature sensors (clear sky). (From Miner *et al.*, 1972. © American Geophysical Union.)

The possibility of inferring water vapor profiles from atmospheric emission measurements near the water vapor absorption line is complicated by the fact that the distribution of water vapor is not generally known, nor is it constant. Because of these uncertainties, water vapor profiles are only approximate; however, the integrated water vapor can be obtained more accurately. Because liquid water in clouds has different spectral characteristics than water vapor, it is possible to distinguish between liquid water and the integrated water vapor. Attempts have been made to map rainfall rates over the ocean using satellite radiometers, but so far they have not proved very successful (Viezee *et al.*, 1979; Wilheit *et al.*, 1977). The principal problem is a lack of spatial resolution owing to limitations on antenna size. Measurements over land are difficult because the antenna temperature measured by the radiometer is dominated by the brightness temperature of the land and is thus only slightly affected by the presence of rain. The resolution problem can be overcome by going to wavelengths on the order of 3 mm or even shorter. The measurement of rain over land presents a more

serious problem; possibly a radar or IR channel may help to overcome this limitation.

To overcome the inversion limitations described previously, use is made of a priori data. The procedure usually followed is illustrated in Rosenkranz (1982), Staelin *et al.* (1976), Waters *et al.* (1975), Westwater (1965). It is often referred to as a statistical estimation technique that consists of a regression analysis of atmospheric temperature profiles and numerically calculated atmospheric emission. The atmospheric temperature, represented by the vector **T**, is related to the measured brightness temperatures $\mathbf{T_B}$ by the matrix **D**:

$$\mathbf{T} = \mathbf{D} \cdot \mathbf{T_B}. \tag{40}$$

The elements of the matrix are derived from a priori data. For example, a large set of previously measured radiosonde profiles that are representative of the region of interest are collected. Brightness temperatures for each of these profiles are then calculated for a set of frequencies. Using a least-squares regression approach, a **D** matrix that produces the best agreement between the "true" temperatures measured with radiosondes and the inferred temperatures is derived. This **D** matrix is then used to calculate a vertical temperature profile from a set of brightness temperature measurements. Different **D** matrices may be used for different locations, seasons, etc. The complexity of the matrix may range from completely linear, with Gaussian statistics, to nonlinear. More sophisticated methods using spatial filtering concepts have also been employed (Rosenkranz, 1982).

1. *Satellite Radiometry*

Probably the most successful application to date of millimeter-wave remote sensing has been the determination of meteorological profiles from a satellite (Staelin, 1981). The groundwork for temperature sensing was provided by Meeks and Lilley (1963) when they calculated the weighting functions for oxygen. The idea of obtaining water vapor profiles was first proposed by Barrett and Chung (1962). These pioneering efforts were followed by measurements from a balloon (Barrett *et al.*, 1966), from an aircraft (Rosenkranz *et al.*, 1972), and finally from the Nimbus-5 and Nimbus-6 experimental satellites (Staelin *et al.*, 1977; Waters *et al.*, 1975). Millimeter-wave radiometers are now used on the Tiros-N and military DMSP operational satellites. It is expected that in the latter 1980s radiometers having as many as 15 or 20 channels will be employed.

a. *Temperature Profiles.* The caliber of temperature profiles that can be obtained from a satellite is illustrated by examining the results from the Nimbus-5 (Nimbus-E) Microwave Spectrometer (NEMS) (Waters *et al.*,

1975). A five-channel radiometer was employed; frequencies of 53.65, 54.9, and 58.8 GHz were used to sense the temperature, and frequencies of 22.235 and 31.4 GHz were used to sense water vapor and liquid water, respectively. Temperatures were retrieved for heights corresponding to pressure levels of 1000, 850, 700, 500, 400, 300, 250, 200, 150, and 100 mbars, so comparisons could be made between the inferred temperatures and those provided by the National Meteorological Center (NMC) obtained from radiosondes and commercial aircraft. Eighty-two pairs of temperature profiles obtained from NEMS and NMC were compared. The results show average temperature differences of 2.1 K for measurements conducted in June and 1.6 K for those conducted in December. These differences would probably have been slightly smaller if the effects of clouds had been taken into account (Staelin *et al.*, 1975). It should be emphasized that discrepancies are also likely to arise because the NEMS temperature is averaged over a surface area of approximately 200 × 300 km, whereas the radiosonde is a point measurement; also, the measurements were not taken at exactly the same time.

b. *Water Vapor and Liquid Water Content.* As mentioned previously, it is more difficult to infer water vapor profiles than temperature profiles from atmospheric emission measurements because of the spatial and temporal variations in the water vapor. However, approximate water vapor profiles and more accurate integrated water vapor abundances have been obtained. Although the 22.235-GHz water vapor resonance is the principal resonance below 50 GHz, it is relatively weak, and thus the total emission at that frequency can be influenced by liquid water emission. Cloud liquid water emission, however, is essentially nonresonant, so it can be distinguished from water vapor by a measurement off the water vapor line. The weakness of the water vapor line does, however, produce a serious problem, namely, the contribution from the earth's surface. Because land has an emissivity typically in the range 0.8–1.0, its brightness temperature is almost equal to its surface temperature. Thus, small contributions from the water vapor emission are dominated by the earth background and are not strong enough to be used for inferring water vapor data. For this reason water vapor and liquid water abundances can be inferred only from measurements over water that has an emissivity of about 0.45 at millimeter wavelengths and thus presents a cool background. The 183-GHz water vapor resonance may be better suited for measurements over land, because it is much stronger than the 22.235-GHz resonance. In addition, it has the potential of producing improved water vapor profiles, because it would result in better vertical resolution.

The state of the art of inferring water vapor and liquid water abundances

using satellite radiometry, as for temperature, is best illustrated by reviewing the NEMS results (Staelin *et al.*, 1976). As mentioned previously, 22.235- and 31.4-GHz channels were used. The abundance of water vapor in the atmosphere was inferred from a linear combination of the brightness temperatures at the two frequencies. The coefficients of the brightness temperatures were obtained using a multidimensional regression analysis based on brightness temperatures computed for about 150 radiosonde profiles. The liquid water estimates were also based on a linear combination of the two brightness temperatures. The comparison of radiometric-derived and radiosonde water vapor and liquid water is difficult because they are not for identical regions, nor were they measured at exactly the same time.

With this limitation in mind, the accuracy of the water vapor estimates was tested by comparison with 31 sets of radiosonde data collected throughout the Northern Hemisphere during a 2-year period. It was concluded that integrated abundances of water vapor and liquid water had estimated NEMS accuracies of 0.2 and 0.01 g/cm^2, respectively. It is expected that improved results could be obtained by using additional frequencies.

2. *Ground-Based Radiometry*

From an applications standpoint, ground-based radiometric sensing has not progressed as rapidly as satellite radiometric sensing. Although, in principle, comparable meteorological profiles should be achievable with ground-based systems, particularly near the ground, they are not capable of readily obtaining global data. For temperature profiling there is a distinct difference between upward- and downward-directed systems, as was seen in Figs. 22 and 23. The upward-directed weighting functions are approximately exponential and all peak at the surface. For this reason the best accuracy is achieved at low altitudes and the accuracy gradually diminishes at higher altitudes. Temperature profiles are particularly important at very low altitudes because it is at these levels that temperature inversions often occur, and the ability to detect the presence of an inversion layer is very useful. Water vapor and liquid water ground-based systems are valuable because they are operable over land as well as water; this has not yet been achieved with satellite systems. Thus it is expected that ground-based radiometry will ultimately also be used for operational meteorological sensing.

a. *Temperature Profiles.* The procedure for obtaining temperature profiles with ground-based radiometers is very similar to that used for satellite radiometers. The state of the art of this technique can be illustrated by the controlled experiment conducted by Decker *et al.* (1978). Eighty-eight simultaneous rawinsonde and radiometer-derived profiles were measured under both clear and cloudy conditions at locations in Pt. Mugu,

California, and the Gulf of Alaska. A five-channel radiometer with temperature profiling frequencies of 52.85, 53.85, and 55.45 GHz and water vapor and liquid water frequencies of 22.235 and 31.65 GHz was utilized. Assuming the radiosonde temperatures are correct (not necessarily a valid assumption), the rms deviations between rawinsonde and radiometric-derived temperatures ranged from 1.1 K at heights within about 1 km of the surface to 2.8 K at a height of about 12 km. These accuracies compared well with the predicted accuracies and are considered acceptable for numerical weather prediction.

b. *Water Vapor and Liquid Water Content.* The same experiment was used to retrieve water vapor profiles and total precipitable water. The agreement between the rawinsonde and radiometric-derived water vapor profiles was not as good as predicted; it is believed that the uncertainty in the absorption coefficient of water vapor could be a significant source of error (Westwater, 1978). Although there was general agreement in the total precipitable waters of the two methods, the rms difference of 0.32 cm was about 0.1 cm larger than predicted. A problem that arises in inferring the liquid water content of a cloud is that a cloud temperature must be assumed and an error in this temperature can produce a large error in the estimated liquid water, which in turn produces an error in the vapor measurement. In an effort to obtain a more accurate integrated liquid water content, an absorption measurement was made in addition to the emission measurements (Snider *et al.*, 1980). The absorption was measured at a frequency of 28.56 GHz using the beacon on the COMSTAR satellite (Cox, 1978). By combining the absorption measurement with the brightness temperature, it is believed that a more accurate liquid water content can be obtained. Because it is very difficult to obtain independent liquid water contents of clouds, the expected improvement in utilizing an absorption measurement has not been confirmed. However, preliminary results seem to be consistent with the liquid contents that would be expected of certain types of clouds, so better accuracies are expected.

C. Radar Sensing

In the earliest days of radar it was quickly recognized that some returns from the atmosphere were meteorologically induced, and since the early 1940s meteorological echoes have been classified and related to synoptic weather conditions. Most of the initial radar meteorological observations were conducted at longer wavelengths because of the availability of high-power radars; in addition, rain was of principal concern and centimeter wavelengths were optimal for rain studies. Later it was realized that cloud sensing could be more effectively accomplished at shorter wavelengths,

because cloud droplets are typically less than 100 μ in diameter and are not easily detectable at centimeter wavelengths. This led to the development of the first millimeter-wave meteorological radar. The development of millimeter-wave radars for cloud studies progressed rather slowly over the years, and only recently are newly designed millimeter-wave Doppler, dual-polarized radars being built to study cloud composition and dynamics.

Although ground-based millimeter-wave radars have not been used for rain studies because they are not as effective as longer-wavelength radars, they do have several features that make them attractive for space-borne precipitation measurements. The principal limitations imposed on space-borne radars are size and weight. To obtain a sufficiently small field of view and minimize ground clutter, very-high-resolution antennas are needed; these are available at millimeter wavelengths, and systems that would operate at these wavelengths are being planned.

Although millimeter-wave radars can be used to infer wind speed, they are not as effective as longer-wavelength systems because the returns are much weaker. Thus it is unlikely that they will be used for this application, unless perhaps the need arises for an airborne system for obtaining very-high-resolution maps of a localized region.

Finally, millimeter-wave radars have great potential in the area of entomology—the study of insects. The movements of insects have been the subject of much research, speculation, and controversy. More quantitative data on insect movement are desperately needed, and millimeter-wave radars are uniquely suited for this application.

In summation, it appears that the most promising applications for millimeter-wave remote sensing radars are in the study of cloud dynamics and entomology. Space-borne millimeter-wave radars for sensing precipitation could prove useful when used in conjunction with longer-wavelength radars or millimeter-wave radiometers.

1. *Cloud Composition*

One of the earliest millimeter-wave radars was the AN TPQ-6, which was used for measuring the heights of cloud bases and tops (Donaldson, 1955). This ultimately evolved into the AN TPQ-11, an 8.6-mm-wavelength, pulse-modulated, two-dish radar capable of providing continuous records of cloud and precipitation height and density (Petrocchi and Paulsen, 1966). Information on wind shear, melting zone, and echo intensity in addition to cloud bases and tops and their trends could also be derived. Later a pseudo-noise coded Doppler 8.6-mm-wavelength radar was developed by Pasqualucci (1970) and used to measure drop size distributions in precipitation and vertical air velocity in both clouds and precipitation. A new

8.6-mm-wavelength Doppler radar with polarization diversity has been built (Pasqualucci, 1981) and is being used to study cloud microphysics, which includes liquid water content, ice crystal versus water drop concentrations, and air motion. More recently, it has been proposed that a Doppler phase-coherent radar be developed to operate at a frequency of 90 GHz (Lhermitte, 1981). An evaluation of the sensitivity characteristics of this radar indicates that it would have enormous potential for the study of clouds in their early stages of development.

2. *Rain Distribution*

Although ground-based rain sensing utilizing radar is generally best accomplished at centimeter wavelengths, a principal problem that arises when attempting this from space is that of antenna size (Atlas and Thiele, 1981). The cell sizes of rain are such that an instantaneous field of view of approximately a few kilometers is necessary. In addition, a narrow beam is needed so that effects of surface clutter can be minimized. For these reasons millimeter-wave radars are being considered for this application. If the radar were designed to operate at a wavelength of about 8 mm, then an antenna with a diameter of 3.4 m would provide 2-km resolution from an 800-km orbit. However, this system would have the limitation that accompanies attenuating radars, namely, the uncertainty that arises because the return signal is attenuated by the rain. This usually makes it necessary to assume that the rain rate is constant as a function of height, which is not necessarily the case.

It has been proposed that the SEASAT altimeter that operates at a wavelength of 2.2 cm (close to millimeter waves) be modified to measure rain rate (Goldhirsh and Walsh, 1982). This is considered a first-step approach, and although the assumption of a constant rain rate with height is considered a weak point, it is believed that meaningful rainfall data could be obtained with a very small investment. It would also provide an excellent opportunity to gain experience in using a millimeter-wave space-borne radar for measuring precipitation on a global scale.

As mentioned previously, there is some merit in considering a hybrid radar–radiometric system for this application. This combination would be particularly useful over the ocean, because the radiometer would provide data on the total attenuation and water content that would be very helpful in the interpretation of the radar returns. Measurements have been made with an airborne radar–radiometer system operating at 10 and 34.5 GHz (Yoshikado *et al.*, 1981). This system was developed as a first step toward a satellite system. The aircraft measurements were compared with those from a ground-based *C*-band radar and the results were encouraging.

3. *Wind Speed*

Wind speed can be inferred from a measurement of the Doppler shift in the frequency of a scattered signal. This may be done with either a monostatic or a bistatic radar. Under clear sky conditions the transmitted signal is scattered by inhomogeneities in the refractive index structure; because these inhomogeneities are moving along with the wind, the Doppler shift produced by this motion is proportional to the wind speed. Under conditions of cloud or precipitation, the scattering is from particulates that are also moving along with the wind. With a monostatic radar, the horizontal components of the wind are generally measured by rotating the antenna in azimuth to obtain wind direction and varying the elevation angle to obtain wind height. The vertical wind component is measured with the antenna pointed toward zenith.

The bistatic system is not as versatile as the monostatic, because winds can be measured only in a fixed direction, unless either the transmitter or receiver is mobile or multiple transmitters and/or receivers are used. Another complication is that the vertical and horizontal components are not easily resolved. For the horizontal crosspath component the Doppler shift is zero when the common volume is at the center of the great circle path; it becomes positive when the common volume is moved to the side of the great circle path in the upwind direction and negative when the common volume is moved to the side in the downwind direction. Thus, the vertical component can be resolved only when the common volume is on the great circle path. The horizontal along-the-path component is very weak compared to the crosspath and therefore more difficult to measure.

Even though the bistatic system is much more limited than the monostatic system, because it can operate only in a fixed direction and does not have the resolution features of the monostatic radar, it has the distinct advantage of being a much more sensitive radar (Lammers, 1973); this is very important at millimeter wavelengths, where power is at a premium.

For the reasons stated, most of the radars that have been used as wind sensors have operated at longer wavelengths (Gage and Balsley, 1978), and the highest frequency at which wind sensing has been done is 15.7 GHz using a forward scatter system (Altshuler *et al.*, 1968; Olsen and Lammers, 1973). At this time the only advantage in using millimeter waves for wind sensing seems to be the feature of being able to obtain higher resolution with smaller mobile antennas.

4. *Insect Detection*

In the early days of radar, unexplained returns from the clear air were classified as clutter or "angels" because these unwanted signals interfered

with the detection of targets. Eventually, it was recognized that these sources of clutter were refractive index inhomogeneities and insects and birds (Atlas, 1959; Crawford, 1949; Hajovsky *et al.*, 1966; Hardy and Katz, 1969). Before long, available radars were used to study insects (Frost, 1971; Glover *et al.*, 1966; Richter *et al.*, 1973; Riley, 1973). Radar has been considered an important tool in the field of entomology (Eastwood, 1967), and a workshop has been held to investigate the potential of radar for insect population ecology and pest management (Vaughn *et al.*, 1979).

As in most emerging fields, existing radars designed for other applications have been used in entomology. The potential of radar for use in entomology now appears so important that the need for optimally designed ground-based and air-borne radars has been substantiated, and millimeter-wave radars are expected to play a key role in this application. Because the dielectric properties of insects depend mostly on body moisture, the maximum target cross-section should occur when the wavelength is comparable to the circumference of the insect. Many insects have sizes on the order of millimeters, so millimeter radars should be optimal, particularly for tracking single insects at short ranges. Longer-wavelength radars could still be used for tracking swarms of insects at long ranges. Because the operational aspects of pest management may encompass regions of millions of square miles in extent, air-borne radars will be needed and millimeter-wave systems have desirable characteristics for this application.

V. Conclusion

The interaction of millimeter waves with atmospheric gases and particulates has been examined. Precipitation in general and rain in particular limit the performance of longer millimeter-wave systems. Systems operating at short millimeter wavelengths are significantly affected by high water vapor absorption in addition to precipitation, so applications in this region of the spectrum will of necessity be limited to very short paths. In the area of remote sensing, most applications will also use longer millimeter wavelengths.

The use of millimeter waves has probably not progressed as rapidly as had been originally anticipated. For many years, the more optimistically inclined envisioned millimeter waves revolutionizing the traditionally longer-wavelength communications and radar systems and traditionally shorter-wavelength remote sensing systems. When the discovery of the laser created a temporary lull in millimeter-wave research, the more pessimistically inclined feared that millimeter waves had passed from infancy to obsolescence without having experienced a period of fruitfulness. Finally, there were realists who recognized that cost is a major consideration and that

millimeter-wave systems would reach the marketplace only when they could be shown to be competitive with systems that operate at longer or shorter wavelengths or to have unique properties such that needed applications could be realized only with millimeter waves. So far, history seems to be supporting the realists.

References

Altshuler, E. E. (1968). *Microwave J.* **11,** 38–42.

Altshuler, E. E. (1971). AFCRL Report 71-0419, AD73 1170, National Technical Information Service, Springfield, Virginia.

Altshuler, E. E., and Mano, K. (1982). Rpt. No. RADC-TR-82-7, National Technical Information Service, Springfield, Virginia.

Altshuler, E. E., and Telford, L. E. (1980). *Radio Sci.* **15,** 781–796.

Altshuler, E. E., Lammers, U. H. W., Day, J. W., McCormick, K. S. (1968). *Proc. IEEE* **56,** 1728–1731.

Altshuler, E. E., Gallop, M. A., and Telford, L. E. (1978). *Radio Sci.* **13,** 839–852.

Atlas, D. (1959). *J. Atmos. Terr. Phys.* **15,** 262–287.

Atlas, D., Kerker, M., and Hitschfeld, W. (1953). *J. Atmos. Terr. Phys.* **3,** 108–119.

Atlas, D., and Thiele, O. W. (1981). NASA Workshop Rpt. Precipitation Measurements from Space, Goddard Lab. for Atmos. Sci., Greenbelt, Maryland.

Barrett, A. H., and Chung, V. K. (1962). *J. Geophys. Res.* **67,** 4259–4266.

Barrett, A. H., Kuiper, J. W., and Lenoir, W. B. (1966). *J. Geophys. Res.* **71,** 4723–4734.

Battan, L. J. (1973). "Radar Observations of the Atmosphere." Univ. of Chicago Press, Chicago, Illinois.

Bean, B. R., and Dutton, E. J. (1968). "Radio Meteorology." Dover, New York.

Blomquist, A., and Norbury, J. R. (1979). *Alta Freq.* **66,** 185–190.

Booker, H. G., and Gordon, W. E. (1950). *Proc. IRE* **36,** 401–412.

Brussard, G. (1976). *IEEE Trans. Antennas Propag.* **24,** 5–11.

CCIR (1978). "Propagation Data Required for Transhorizon Radio Relay Systems." Rpt. 238-3, V, pp. 199–215.

CCIR (1982a). "Attenuation by Atmospheric Gases." Rpt. 719 (Mod I), V.

CCIR (1982b). "Attenuation and Scattering by Precipitation and Other Atmospheric Particles." Rpt. 721 (Mod I), V.

Chu, T. S. (1979). *Bell Syst. Tech. J.* **58,** 549–555.

Cox, D. C. (1978). *Bell Syst. Tech. J.* **57,** 1231–1255.

Crane, R. K. (1973). Tech. Rpt. 498, Lincoln Lab, MIT, Lexington, Massachusetts.

Crane, R. K. (1980a). ERT-Doc. P-A502, Environ. Res. and Technol., Inc., Concord, Massachusetts.

Crane, R. K. (1980b). *IEEE Trans. Commun.* **28,** 1717–1733.

Crane, R. K. (1981). *Radio Sci.* **16,** 649–669.

Crawford, A. B. (1949). *Proc. IRE* **37,** 404–405.

Davies, P. G. (1973). *IEE Conf. Publ.* **98,** 141–149.

Decker, M. T., Westwater, E. R., and Guirand, F. O. (1978). *J. Appl. Meteorol.* **17,** 1788–1795.

Donaldson, R. J. Jr. (1955). *J. Meteorol.* **12,** 238–244.

Eastwood, E. (1967). "Radar Ornithology." Methuen, London.

Eldridge, R. G. (1966). *J. Atmos. Sci.* **23,** 605–613.

Elgered, G. K. (1982). *IEEE Trans. Antennas Propag.* **30,** 502–505.

Falcone, V. J., Abreu, L. W., and Shettle, E. P. (1979). Rpt. No. AFGL-TR-79-0253, National Technical Information Service, Springfield, Virginia.
Fante, R. L. (1980). *Proc. IEEE* **68,** 1424–1442.
Friis, H. T., Crawford, A. B., and Hogg, D. C. (1957). *Bell Syst. Tech. J.* **36,** 627–644.
Frost, E. (1971). *Proc. Seventh Int. Symp. Remote Sensing Environ.* **7,** 1909–1915.
Furuhama, Y., and Ihara, T. (1981). *IEEE Trans. Antennas Propag.* **29,** 275–281.
Gage, K. S., and Balsley, B. B. (1978). *Bull. Am. Meteorol. Soc.* **59,** 1074–1093.
Gallagher, J. J., McMillan, R. W., Rogans, R. C., and Snider, D. E. (1980). U.S. Army Missile Command Rpt., RR-80-3, Redstone Arsenal, AL 35809, 100–108.
Gallop, M. A., Jr., and Telford, L. E. (1975). *Radio Sci.* **11,** 935–945.
Glover, K. M., Hardy, K. R., Konrad, T. G., Sullivan, W. N., and Michaels, A. S. (1966). *Science* **154,** 967–972.
Goldhirsh, J. (1979). *IEEE Trans. Geosci. Electron.* **17,** 218–239.
Goldhirsh, J., and Walsh, E. J. (1982). *IEEE Trans. Antennas Propag.* **30,** 726–733.
Gough, M. W. (1968). *IEE Conf. Publ.* **48,** 93–100.
Haakinson, E. J., Violette, E. J., and Hufford, G. A. (1980). NTIA Report 80-35, U.S. Dept. of Commerce, NTIA.
Hajovsky, R. G., Deam, A. P., and LaGrone, A. H. (1966). *IEEE Trans. Antennas Propag.* **14,** 224–227.
Hall, M. P. M. (1979). "Effects of the Troposphere on Radio Communication." Peregrinus Ltd., New York.
Hardy, K. R., and Katz, I. (1969). *Proc. IEEE* **57,** 468–480.
Hayes, D. H., Lammers, U. H. W., Marr, R. A., and McNally, J. J. (1979). *EASCON Rec.* **2,** 362–368.
Hogg, D. C. (1980). *Trans. Antennas Propag.* **28,** 281–283.
Hogg, D. C., and Chu, T. S. (1975). *Proc. IEEE* **63,** 1308–1331.
Hooke, W. H., and Hardy, K. R. (1975). *J. Appl. Meteorl.* **14,** 31–38.
Ippolito, L. J. (1981). *Proc. IEEE* **69,** 697–727.
Ishimaru, A., and Cheung, R. L. T. (1980). *Radio Sci.* **15,** 507–516.
Lammers, U. H. W. (1973). *Radio Sci.* **8,** 89–101.
Leuenberger, K., Lee, R. W., Waterman, A. T. (1979). *Radio Sci.* **14,** 781–791.
Lhermitte, R. (1981). *20th Conf. Radio Meteorol.* **20,** 744–748.
Lo, L., Fannin, B. M., Straiton, A. W. (1975). *IEEE Trans. Antennas Propag.* **23,** 782–786.
Mano, K., and Altshuler, E. E. (1981). *Radio Sci.* **16,** 191–195.
McCormick, K. S. (1972). *IEEE Trans. Antennas Propag.* **20,** 747–755.
Medhurst, R. G. (1965). *IEEE Trans. Antennas Propag.* **13,** 550–563.
Meeks, M. L., and Lilley, A. E. (1963). *J. Geophys. Res.* **68,** 1683–1703.
Mie, G. (1908). *Ann. Phys.* **25,** 377–445.
Miner, G. F., Thornton, D. D., and Welch, W. J. (1972). *J. Geophys. Res.* **77,** 975–991.
Olsen, R. L. (1981). *Radio Sci.* **16,** 631–647.
Olsen, R. L., and Lammers, U. H. W. (1973). *IEE Conf. Prop. Radio Waves 10 GHz* **98,** 197–201.
Olsen, R. L., Rogers, D. V., and Hodge, D. E. (1978). *IEEE Trans. Antennas Propag.* **26,** 318–329.
Parl, S. A., and Malaga, A. (1982). Personal communication, Signatron, Inc., Lexington, Massachusetts.
Pasqualucci, F. (1970). *14th Conf. Radar Meteorol.* **14,** 452–455.
Pasqualucci, F. (1981). *20th Conf. Radar Meteorol.* **20,** 646–648.
Petrocchi, P. J., and Paulsen, W. H. (1966). *12th Conf. Radar Meteorol.* **12,** 467–472.

Platt, C. (1970). *J. Atmos. Sci.* **27,** 421–425.
Povejsil, D. J., Raven, R. S., and Waterman, P. (1961). "Airborne Radar." Van Nostrand, Princeton, New Jersey.
Pruppacher, H. R., and Pitter, R. L. (1971). *J. Atmos. Sci.* **28,** 86–94.
Rafuse, R. P. (1981). Rpt. No. ESD-TR-81-290, Lincoln Lab., Lexington, MA.
Richter, J. H., *et al.* (1973). *Science* **180,** 1176–1178.
Riley, J. R. (1973). *Proc. IEE* **120,** 1229–1232.
Rooryck, M., and Battesti, J. (1975). Rpt. No. SP-113, European Space Agency, Paris, France, pp. 217–227.
Rosenkranz, P. W. (1982). *Radio Sci.* **17,** 245–267.
Rosenkranz, P. W., *et al.* (1972). *J. Geophys. Res.* **77,** 5833–5844.
Rozenberg, V. I. (1972). "Scattering and Attenuation of Electromagnetic Radiation Particles." Hydrometeorological Press, Leningrad, USSR.
Rummler, W. D. (1979). *Bell Syst. Tech. J.* **58,** 1037–1071.
Ryde, J. W., and Ryde D. (1945). General Electricity Company Rpt. No. 8670, Wembley, England.
Sandberg, J. (1980). *IEEE Trans. Antennas Propag.* **28,** 743–750.
Schaper, L. W., Jr., Staelin, D. H., and Waters, J. W. (1970). *Proc. IEEE* **58,** 272–273.
Shen, L. C. (1970). *Trans. Antennas Propag.* **18,** 493–497.
Skolnik, M. I. (1970). NRL Rpt. 2159, NRL, Washington, D.C.
Slobin, S. D. (1982). *Radio Sci.* **17,** 1443–1454.
Smith, E. K. (1982). *Radio Sci.* **17,** 1455–1464.
Smith, E. K., and Weintraub, S. (1953). *Proc. IRE.* **41,** 1035–1037.
Snider, J. B., Burdick, H. M., and Hogg, D. C. (1980). *Radio Sci.* **15,** 683–693.
Staelin, D. H. (1981). *Trans. Antennas Propag.* **29,** 683–687.
Staelin, D. H., *et al.* (1975). *J. Atmos. Sci.* **32,** 1970–1976.
Staelin, D. H., Kunzi, K. F., Pettyjohn, R. L., Poon, R. K. L. and Wilcox, R. W. (1976). *J. Appl. Meteorol.* **15,** 1204–1214.
Staelin, D. H., Rosenkranz, P. W., Borath, F. T., Johnston, E. J., and Waters, J. W. (1977). Science **197,** 991–993.
Stephanson, E. T. (1981). *Radio Sci.* **16,** 608–629.
Stewart, D. A. (1980). Rpt. RR-8D-3, Proc. of Workshop on Millimeter and Submillimeter Atmospheric Propagation Applicable to Radar and Missile Systems, U.S. Army Missile Command, Redstone Arsenal, AL, 77–82.
Strickland, J. I. (1974). *J. Rech. Atmos.* **8,** 347–358.
Strobehn, J. W. (1968). *Proc. IEEE* **56,** 1301–1318.
URSI Commission F Working Paper (1981). Radio Sci. **16,** 825–829.
Van de Hulst, H. C. (1957). "Light Scattering by Small Particles." Wiley, New York.
Vander Vorst, A. (1979). *Alta Freq.* **48,** 201–209.
Vaughn, C. R., Wolf, W., and Klassen, W. (1979). Radar, Insect Population Ecology, and Pest Management, NASA CP-2070, Wallops Flight Center, Wallops Island, Virginia.
Viezee, W., Shigeishu, H., and Chang, A. T. C. (1979). *J. Appl. Meteorol.* **18,** 1151–1157.
Waterman, A. T., Jr. (1958). *Proc. IRE* **46,** 1842–1848.
Waters, J. W. (1976). "Methods of Experimental Physics." **12B,** Chapter 23. Academic Press, New York.
Waters, J. W., Kunzi, K. F., Pettyjohn, R. L., Poor, R. K. L., and Staelin, D. H. (1975). *J. Atmos. Sci.* **32,** 1953–1969.
Westwater, E. R. (1965). *Radio Sci. J. Res.* NBS/USNC-URSI **69D,** 1201–1211.
Westwater, E. R. (1976). ESSA Tech. Rpt. IER 30-ITSA 30, National Technical Information Service, Springfield, Virginia.

Westwater, E. R. (1978). *Radio Sci.* **13,** 677–785.
Wilheit, T. T., Chang, M. S. V., Rao, E. B., Rogers, E. B., and Tyson, J. S. (1977). *J. Appl. Meteorol.* **16,** 551–560.
Wilson, R. W., (1969). *Bell Syst. Tech. J.* **48,** 1383–1404.
Wu, S. C. (1979). *IEEE Trans. Antenna Propag.* **27,** 233–239.
Wulfsberg, K. N. (1967). *Radio Sci.* **2,** 319–324.
Yoshikado, S., *et al.* (1981). *20th Conf. Radar Meteorol.* **20,** 287–294.
Zavody, A. M. (1974). *Proc. IEE* **121,** 257–263.

MISSION
of
Rome Air Development Center

RADC plans and executes research, development, test and selected acquisition programs in support of Command, Control Communications and Intelligence (C^3I) activities. Technical and engineering support within areas of technical competence is provided to ESD Program Offices (POs) and other ESD elements. The principal technical mission areas are communications, electromagnetic guidance and control, surveillance of ground and aerospace objects, intelligence data collection and handling, information system technology, ionospheric propagation, solid state sciences, microwave physics and electronic reliability, maintainability and compatibility.

Printed by
United States Air Force
Hanscom AFB, Mass. 01731